Mitochondrial Phosphopantetheinylation is Required for Oxidative Function

Pieter R. Norden[1,*], Riley J. Wedan[1,*], Jacob Z. Longenecker[1], Samuel E. J. Preston[1], Naomi Graber[1], Olivia Ols[1], Morgan Canfield[1], Elizabeth McLaughlin[1], and Sara M. Nowinski[1]

[1]Department of Metabolism and Nutritional Programming, Van Andel Institute, Grand Rapids, MI

*These authors contributed equally

Correspondence:
Sara.nowinski@vai.org (S.N.)

Abstract

Sub-cellular compartmentalization of metabolism has important implications for the local production of metabolites and redox co-factors, as well as pathway regulation. 4'-phosphopantetheinyl (4'PP) groups are essential co-factors derived from coenzyme A and added to target proteins in both the cytoplasm and mitochondria by phosphopantetheinyl transferase (PPTase) enzymes. Mammals express only one PPTase, thought to localize to the cytoplasm: aminoadipate semialdehyde dehydrogenase phosphopantetheinyl transferase (AASDHPPT); raising the question of how mitochondrial proteins are 4'PP-modified. We found that AASDHPPT is required for mitochondrial respiration and oxidative metabolism via the mitochondrial fatty acid synthesis (mtFAS) pathway. Moreover, we discovered that a pool of AASDHPPT localizes to the mitochondrial matrix via an N-terminal mitochondrial targeting sequence contained within the first 13 amino acids of the protein. Our data show that mitochondrial localization of AASDHPPT is required to support mtFAS function, and further identify two variants in *Aasdhppt* that are likely pathogenic in humans.

Keywords:
Mitochondria, fatty acid synthesis, electron transport chain, reductive carboxylation, metabolism, respiration, compartmentalization, phosphopantetheine

Abbreviations:
4'PP – 4'-phosphopantetheine/yl, AASDHPPT – aminoadipate semialdehyde dehydrogenase phosphopantetheinyl transferase, ALDH1L2 – Aldehyde Dehydrogenase 1 Family Member L2, CoA – coenzyme A, DHRS2 – mitochondrial Dehydrogenase/Reductase 2, ETC – electron transport chain, FAS – fatty acid synthesis, FASN – fatty acid synthase, LYRM – leucine tyrosine arginine motif, mtFAS – mitochondrial fatty acid synthesis, NAD^+ - nicotinamide adenine dinucleotide (oxidized form), OGDH – oxoglutarate dehydrogenase, PAGE – polyacrylamide gel electrophoresis, PDH – pyruvate dehydrogenase, PPT – mammalian AASDHPPT, PPTase – phosphopantetheinyl transferase, PTM – posttranslational modification, SDHB – succinate dehydrogenase subunit B, TCA – tricarboxylic acid, VUS – variant of uncertain significance

Introduction

Mitochondria are well known for their ability to perform oxidative metabolism and produce cellular energy via the citric acid (TCA) cycle and the electron transport chain (ETC). The ability of mitochondria to perform these functions relies heavily on the transcriptional regulation of nuclear genes that encode mitochondrially localized proteins which participate in these pathways[1]. As a double-membraned organelle, proteins localized to the mitochondria often participate in the same biochemical reactions as proteins localized in the cytoplasm, but are encoded by separate genes[2,3]. These genes often perform essential functions to underpin biological processes that are independent from their cytosolic counterparts. Several examples of parallel enzymatic pathways in the mitochondria and cytoplasm exist, and have been shown to have specific and distinct roles in both metabolism and the metabolic control of cell behaviors[4,5].

4'-phosphopantentheinylation is an essential post translational modification (PTM) whereby a 4'-phosphopantetheine (4'PP) group, derived from coenzyme A (CoA), is covalently attached to both mitochondrial and cytosolic target proteins by a phosphopantetheinyltransferase (PPTase) enzyme[6]. The yeast *Saccharomyces cerevisae* have at least three PPTases: 1) the PPTase domain of Fas2, a subunit of the yeast cytosolic fatty acid synthase, 2) Ppt1, another cytoplasmic PPTase, and 3) Ppt2, which localizes to the mitochondrial matrix[3]. Loss of Ppt2 cannot be compensated for by the cytoplasmic PPTases, providing strong evidence for the compartmentalization of this reaction in yeast[7]. In mammalian genomes, however, there is only one annotated PPTase: aminoadipate-

69 semialdehyde dehydrogenase- phosphopantetheinyl transferase (AASDHPPT), which is
70 thought to exist solely in the cytoplasm[8].
71 A total of six proteins in the mammalian proteome have been found to have a 4'-PP-
72 modified serine, and all have been assumed to be catalyzed by AASDHPPT[6]. However, three
73 of these six proteins are localized to the mitochondria: NADH:Ubiquinone Oxidoreductase
74 Subunit AB1 (NDUFAB1), Aldehyde Dehydrogenase 1 Family Member L2 (AL1L2), and
75 mitochondrial Dehydrogenase/Reductase 2 (DHRS2). Of these three, NDUFAB1, also known
76 as the mitochondrial acyl carrier protein (mtACP), is unique because its functions are essential
77 for life and it requires a 4'PP PTM to carry out these functions[9–11].
78 NDUFAB1 is a structural subunit of complex I of the ETC, as well as an integral part of the
79 mitochondrial fatty acid synthesis (mtFAS) pathway. mtFAS builds *de novo* fatty acyl chains
80 on NDUFAB1, which acts as a soluble scaffold for the new fatty acid in the mitochondrial
81 matrix. As this newly synthesized fatty acid is added to the terminal sulfhydryl group of the
82 4'PP, the addition of a 4'PP group to NDUFAB1 is absolutely necessary for mtFAS to occur[9].
83 Once synthesized, acyl chains built by mtFAS can be donated to the lipoic acid synthesis
84 machinery, which further modify the fully saturated fatty acid created by mtFAS to make lipoic
85 acid (LA)[12]. LA is an essential cofactor for alpha-keto acid dehydrogenases such as pyruvate
86 dehydrogenase and alpha-ketoglutarate dehydrogenase in the TCA cycle. Alternatively, if not
87 donated to lipoic acid machinery, longer acyl chains on NDUFAB1 facilitate interactions with
88 ETC assembly factors to support ETC complex assembly[13]. The yeast mtACP can interact
89 with ETC assembly factors without an acyl chain, but a 4'PP group is essential and may
90 provide a different regulatory signal depending on the presence or absence of an acyl chain[9].
91 NDUFAB1 is therefore central to two major arms of mitochondrial oxidative metabolism: TCA
92 cycle activity through lipoic acid, and ETC assembly through protein-protein interactions.
93 Despite this pivotal role, how NDUFAB1 is activated with its 4'PP group in mammals is still
94 unclear.
95 Because yeast have a dedicated mitochondrial PPTase, we questioned whether an
96 unidentified PPTase gene existed in mammals, or conversely if AASDHPPT was important for
97 mitochondrial function regardless of its reported cytoplasmic localization. One prior study has
98 demonstrated that AASDHPPT is sufficient to add a 4'PP group to NDUFAB1 *in vitro*[8]. We
99 therefore set out to understand if AASDHPPT was required for mitochondrial function *in vivo*
100 and, if so, how it modifies mitochondrial targets like NDUFAB1 despite existing in separate
101 cellular compartments. To do so, we created clonal mouse skeletal myoblast (C2C12) cell
102 lines with hypomorphic mutations in AASDHPPT, and discovered that AASDHPPT was

103 necessary for mitochondrial respiration and oxidative metabolism due to its action on
104 NDUFAB1 and downstream effects on the mtFAS pathway. Furthermore we found, contrary
105 to prior reports, that a pool of endogenous AASDHPPT localized to the mitochondrial matrix
106 via an N-terminal mitochondrial targeting sequence. Our data suggest that this previously
107 undescribed mitochondrial localization of AASDHPPT is required for mtFAS and mitochondrial
108 oxidative function.
109
110 **Results**
111
112 **AASDHPPT is a major determinant of mitochondrial oxidative function**
113 To test whether AASDHPPT (hereafter abbreviated PPT) is required for mitochondrial
114 oxidative function, we used a CRISPR/Cas-9-based strategy to mutate *Aasdhppt* in C2C12
115 mouse skeletal muscle myoblasts. Similar to our previous experiences attempting to knockout
116 mtFAS genes in this cell line[13], no complete null clones were generated, however we were
117 able to expand two clonal cell lines with hypomorphic mutations in *Aasdhppt* (Supplemental
118 Figure S1A) that resulted in decreased PPT expression (PPT-1 and PPT-2, Figure 1A). We
119 next investigated whether PPT deficiency resulted in altered respiratory-dependent growth by
120 performing proliferation assays in cell culture media containing either glucose or galactose,
121 the latter requiring functional mitochondrial respiration. Clonal mutant PPT-2 showed
122 significantly reduced growth in glucose media at 72 hours (Figure 1B, Supplemental Figure
123 S1B), while clonal mutant PPT-1 showed a modest, yet non-statistically significant, reduction
124 in growth compared to control cells. In contrast, both PPT mutants showed markedly reduced
125 proliferation in galactose-containing media (Figure 1C, Supplemental Figure S1B). We next
126 performed a Seahorse mitochondrial stress test in high glucose medium and observed that
127 PPT-deficient mutants exhibited a reduction in both basal respiration rate and spare
128 respiratory capacity compared to controls (Figure 1D). To assess whether PPT-deficient
129 respiratory function was associated with perturbed OXPHOS complex expression and
130 assembly, we performed blue-native PAGE analysis on isolated mitochondria from PPT-
131 deficient and control cells. PPT-deficient mutants displayed reduced levels of fully assembled
132 ETC complex I (CI), complex II (CII) and complex IV (CIV) (Figure 1E). Complex V (CV) was
133 largely unaffected, with only a modest reduction observed in clonal PPT-2 mutant cells.
134 Additionally, complex III (CIII) was not affected by PPT-deficiency but reductions in CIII-
135 containing supercomplexes (SC) were observed (Figure 1E). Together, these data
136 demonstrate that PPT deficiency results in dysfunctional mitochondrial respiratory and ETC

137 assembly phenotypes similar to those of yeast and skeletal muscle myoblasts with impaired
138 mtACP acylation[9,13].
139 As we observed reduced proliferative activity in galactose media alongside a loss of ETC
140 assembly, we hypothesized that nutrient oxidation by the mitochondria would likely be altered
141 in PPT-deficient cells. Therefore, to assess the activity of the TCA cycle we cultured cells in
142 fully labeled ^{13}C-glutamine for up to 6 hours and evaluated carbon entry into TCA cycle
143 intermediates to assess reductive (blue) versus oxidative (red) use of glutamine (Figure 1F).
144 At steady state, PPT-deficient cells demonstrated an increase in the pool size of succinate
145 and a decrease in downstream metabolites such as fumarate, malate, and aspartate (Figure
146 1G, Supplemental Figure S1C-E). Pool sizes of citrate and α-ketoglutarate were variable
147 (Supplemental Figure S1F and G). However, the ratio of malate to citrate is consistently
148 reduced in PPT mutants compared to controls (Figure 1H). The reduction of TCA metabolites
149 downstream of succinate relative to citrate suggests a block in oxidative (NAD^+ consuming)
150 TCA cycle activity.
151 To assess whether this was due to a loss of oxidation of glutamine, citrate labeling
152 patterns were plotted. Citrate M+4 results from the oxidation of glutamine to oxaloacetate and
153 consumes NAD^+, whereas Citrate M+5 results from the reductive carboxylation of glutamine
154 to citrate and regenerates NAD^+. PPT-deficient cells had a reduction in M+4 citrate and an
155 increase in M+5 citrate compared to controls, indicating increased reductive carboxylation of
156 glutamine (Figure 1I). This is further supported by the increase in the ratio of citrate M+5:citrate
157 M+4 at isotopic steady state (Figure 1J).
158 Citrate produced in the mitochondria can also be transported to the cytosol to be broken
159 down by ATP-citrate lyase (ACLY) into malate and acetyl-CoA, with citrate M+4 producing
160 malate M+4 and citrate M+5 producing malate M+3 (Figure 1F). PPT-deficient cells displayed
161 a reduction in malate M+4, which likely results from the loss of M+4 citrate (Figure 1K).
162 However, the PPT-deficient cells did not display a concordant increase in M+3 malate,
163 indicating that differences in malate labeling patterns result from mitochondrial malate, and
164 conversion of citrate to malate in the cytosol is similar or reduced in PPT mutants (Figure 1K).
165 One possibility as to why ACLY activity appears to be similar or decreased in PPT-deficient
166 cells may relate to a loss of PPT's action on cytosolic fatty acid synthase (FASN), which likely
167 lowers consumption of cytosolic acetyl-CoA. In sum, the glutamine labeling patterns in PPT-
168 deficient cells support the loss of oxidative metabolism in the mitochondria, with an increase
169 in the reductive carboxylation of glutamine that is typical of cells with loss of ETC activity[14].
170

171 **AASDHPPT is required for mtFAS**

172 As *Aasdhppt* was clearly important for mitochondrial oxidative function, we next asked
173 which mitochondrial targets were likely to be most prominently involved in this phenotype. As
174 mentioned above, there are six known 4'PP-modified proteins in mammals, three of which are
175 localized within the mitochondria[6]. To explore which of these putative targets displayed the
176 strongest genetic relationships to PPT, we analyzed gene co-dependency relationships from
177 genome-wide CRISPR screens conducted by the DepMap project[15], using the DepMap Public
178 23Q4+ Score Chronos dataset, as an effective method to identify gene functionality within the
179 same biological pathway[16]. Gene effect score comparison between *AASDHPPT* and
180 *NDUFAB1* showed a positive correlation (Pearson r = 0.24) (Figure 2A), whereas non-
181 significant or negative correlations were identified with the genes encoding the two other
182 mitochondrial phosphopantetheinylated proteins, *ALDH1L2* (Pearson r = 0.04) and *DHRS2*
183 (Pearson r = -0.12), respectively (Figure 2B and C). Additionally, *AASDHPPT* gene effect
184 scores showed a similar positive correlation with *FASN* as to *NDUFAB1* (Pearson r = 0.25)
185 whereas the genes encoding other cytoplasmic 4'PP-modified proteins, aminoadipate-
186 semialdehyde dehydrogenase (*AASDH*) and aldehyde dehydrogenase 1 family member L1
187 (*ALDH1L1*), were also non-significant (Supplemental Figure S2A-C).

188 Of note, we observed that the mtFAS pathway gene *OXSM* ranked third overall for co-
189 dependency with *AASDHPPT* (Pearson r = 0.42)[17] out of all genes in the Depmap database
190 (Figure 2D). Additional mtFAS pathway genes also ranked highly in terms of Aasdhppt co-
191 dependency, including *MCAT* and *MECR,* which like *OXSM* showed postive correlation scores
192 that were stronger than that of *NDUFAB1* or *FASN* (Pearson r = 0.36 and 0.32 respectively)
193 (Supplemental Figure S2D and E). Given that the 4'-PP modification is necessary for acyl
194 synthesis on NDUFAB1, these data suggested to us that impaired mitochondrial respiration
195 and TCA cycle metabolism in PPT-deficient cells may be primarily attributable to altered
196 mtFAS function.

197 To further explore the genetic relationships between *AASDHPPT* and mtFAS, we
198 performed clustering and two-dimensional mapping analysis of pairwise correlations of gene
199 essentiality scores with *AASDHPPT*. We included the genes that encode known
200 phosphopantetheinylated proteins, mtFAS pathway genes, downstream genes that encode
201 proteins involved in lipoic acid synthesis and ETC assembly - such as the leucine, tyrosine,
202 arginine motif (LYRM) assembly factors which are regulated by mtFAS[13] - as well as genes
203 associated with the GO term "pantothenate metabolism" from the DepMap project database
204 (Figure 2E, Supplemental Figure S2F and G). Clustering analysis of co-dependency

205 correlations showed that mitochondrial and cytosolic fatty acid synthesis (clusters 1 and 2,
206 respectively) were distinctly separated (Supplemental Figure S2F). Two-dimensional mapping
207 of correlation distance then showed that these clusters were linked by *AASDHPPT* (Figure
208 2E). *AASDHPPT* most strongly correlated with mtFAS pathway genes, as well as LYRM family
209 members *NDUFA6* (*LYRM6*) and *NDUFB9* (*LYRM3*). This co-dependency suggested that PPT
210 may act as a critical regulator of mtFAS functional activity.

211 To test this hypothesis, we examined whether PPT-deficiency directly altered known
212 mtFAS pathway endpoints, including protein lipoylation and succinate dehydrogenase subunit
213 B (SDHB) stability, which is a reliable surrogate of the LYRM-dependent ETC assembly
214 mechanism we previously described[13]. PPT-deficient cells exhibited reduced lipoylation of
215 pyruvate dehydrogenase (PDH) and α-ketoglutarate dehydrogenase (OGDH) subunits (DLAT
216 and DLST, respectively) along with reduced stability of SDHB (Figure 2F), similar to the
217 molecular phenotype of mtFAS-deficient cells. 4'PP-modification of NDUFAB1 has been
218 demonstrated by SDS-PAGE of purified proteins, as unmodified apo-mtACP has a lower
219 molecular weight and thus migrates faster than 4'PP-modified holo-mtACP[8]. We found that
220 apo-mtACP accumulated, while holo-mtACP was depleted, in PPT-deficient cells (Figure 2F).

221 PDH and OGDH lipoylation, SDHB stability, and detection of holo-mtACP by SDS-PAGE
222 were all rescued in part by transient retroviral-mediated re-expression of full length
223 AASDHPPT with a C-terminal GFP-Flag tag (PPT-GFP) compared to a control vector
224 expressing mitochondrial-localized DSRed (mtDSRed) (Figure 2G). Additionally, basal
225 respiration and spare respiratory capacity were also both restored by retroviral-mediated
226 expression of PPT-GFP for both PPT-deficient cell lines (PPT-1 + PPT and PPT-2 + PPT,
227 Figure 2H). From these data, we conclude that AASDHPPT is required for 4'-PP modification
228 of NDUFAB1 and, therefore, for downstream mtFAS activity, protein lipoylation, ETC assembly
229 and mitochondrial respiration[11].

230

231 **A pool of AASDHPPT localizes to the mitochondrial matrix**

232 NDUFAB1 is localized within the mitochondrial matrix where it carries out its functions in
233 both *de novo* fatty acid synthesis and as a stable subunit of ETC complex I[18,19]. Previous work
234 has definitively demonstrated PPT activity in the cytoplasm, but it is unclear whether PPT is
235 only active in the cytoplasm, or if it also localizes to mitochondria in order to modify targets in
236 that compartment. To address this question, we performed immunofluorescence staining for
237 endogenous PPT expression and mitochondrial ATP synthase subunit ATP5a as a
238 mitochondrial marker protein (Figure 3A). PPT expression was significantly reduced in PPT-

239 deficient cells compared to controls, with clonal mutant PPT-2 exhibiting a stronger loss of
240 PPT intensity compared to PPT-1 (Figure 3B). Within the cytoplasm, PPT demonstrated a
241 punctate, perinuclear expression pattern that co-localized with ATP5a staining in control cells
242 (Pearson r = 0.60 and 0.62), and which decreased with PPT deficiency (Figure 3C).
243 Additionally, we used Mander's Colocalization Coefficient[20] to measure the fraction of PPT
244 that colocalizes with ATP5a, and conversely, the fraction of ATP5a that colocalizes with PPT.
245 As with Pearson co-localization, we found that PPT signal strongly overlapped with ATP5a in
246 control cells. In PPT-deficient cells, this overlap was only significantly reduced in PPT-2 clonal
247 mutants (Supplemental Figure S3A), characteristic of its strongly reduced fluorescent signal.
248 Conversely, ATP5a overlap with PPT was significantly reduced in both PPT-deficient clones
249 (Supplemental Figure S3B). Additionally, PPT expression was surprisingly observed in the
250 nucleus of some, but not all, cells; a finding that we did not pursue further in the present study
251 but which raises intriguing questions for future work.

252 Next, we performed Western blot analysis of subcellular fractions of control and PPT-
253 deficient clonal mutants. We detected endogenous PPT expression in both mitochondrial and
254 post-mitochondrial supernatant (PMS) fractions, which was reduced in PPT-deficient cells
255 (Figure 3D). We further characterized subcellular localization of PPT-GFP in skeletal
256 myoblasts with immunofluorescent staining of ATP5a. PPT-GFP showed strong signal overlap
257 with ATP5a in addition to nuclear expression and punctate distribution within the cytoplasm
258 (Figure 3E). Together with our immunofluorescence analyses, these data demonstrate that a
259 pool of PPT exhibits mitochondrial localization.

260 We next asked whether this pool of mitochondrially-localized PPT was actually inside the
261 mitochondrial matrix, where NDUFAB1 and the rest of the mtFAS machinery reside. To tackle
262 this question, we first used a Proteinase K protection assay in which intact, isolated
263 mitochondria were treated with increasing concentrations of detergent to permeabilize first the
264 outer mitochondrial membrane (OMM) and later the inner mitochondrial membrane (IMM).
265 Western blotting and comparison to control proteins with known sub-mitochondrial localization
266 thus reveals which sub-compartment of the mitochondria a target protein localizes to. OMM
267 proteins (such as mitofusin 2, Mfn2) are degraded sooner than matrix-localized proteins (such
268 as citrate synthase, CS) (Figure 4A). Blotting for PPT-GFP revealed two bands in whole
269 isolated mitochondria; the top band corresponded to the predicted molecular weight of PPT-
270 GFP, while the lower band ran at the molecular weight of free GFP. The higher molecular
271 weight PPT-GFP band behaved similarly to MFN2, while the lower molecular weight band
272 exhibited a similar pattern to CS (Figure 4A). These data led us to propose a model in which

273 PPT-GFP associates with mitochondria, and is imported into the mitochondrial matrix, where
274 the GFP tag may be proteolytically cleaved, giving rise to the free GFP band in our Proteinase
275 K protection assay.

276 To further test this model using an orthogonal method, we employed a bimolecular
277 fluorescence complementation (BiFC) system[21] to visualize and provide additional confidence
278 in the sub-mitochondrial localization of PPT. We used a split-Venus fluorophore tag system in
279 which the N-terminus of the split-Venus tag (VN, residues 1-172) was attached to either the
280 N- or C-terminus of PPT, while the C-terminus of the split-Venus tag (VC, residues 155-238)
281 was attached to the C-terminus of a sub-mitochondrial localization control protein (MFN2 or
282 CS) or NDUFAB1. This system allows us to observe fluorescent signal only when both halves
283 of the split-Venus tag are able to spatially associate within a compartment[21]. Flow cytometric
284 analysis was performed to quantify Venus fluorescence in each of our BiFC conditions. Cells
285 expressing individual split-Venus constructs (i.e., VC or VN, but not both) were used to
286 determine a background level of fluorescence, against which a true Venus-positive signal
287 could be detected. Using this method, we validated that these single construct cell lines, as
288 expected, were Venus-negative (Figure 4B and C). In cells expressing N-terminally tagged
289 PPT (VN-PPT), positive Venus fluorescence was only detected when co-expressed with
290 MFN2-VC (Figure 4B-D), indicating that N-terminally tagged VN-PPT is mitochondrially
291 associated on the OMM. Opposingly, in cells expressing C-terminally tagged PPT (PPT-VN),
292 Venus signal was observed when co-expressed with either CS-VC or NDUFAB1-VC (Figure
293 4B-D). Together with our Proteinase K assay (Figure 4A), these data provide strong evidence
294 that a pool of PPT indeed localizes to the mitochondrial matrix.

295

296 **Mitochondrial localization of AASDHPPT is required for functional mtFAS**

297 Most mitochondrial proteins are encoded by nuclear genes and are targeted to and
298 imported into mitochondria via an N-terminal mitochondrial targeting sequence (MTS). Most
299 MTS consist of approximately 20 to 40 amino acid residues, and direct proteins destined for
300 the mitochondria to the TIM/TOM complex for import[22]. In addition, our BiFC data showed that
301 tagging PPT on the N-terminus prevented its localization in the mitochondrial matrix (Figure
302 4B-D). We therefore hypothesized that mitochondrial localization of PPT may also be driven
303 by a N-terminal MTS. To test this, we generated truncation constructs lacking the first 13 or
304 36 amino acids of PPT ($PPT_{\Delta 1\text{-}13}$-GFP and $PPT_{\Delta 1\text{-}36}$-GFP), as its amino acid sequence contains
305 two methionine residues downstream of the start codon at positions 14 and 37. Fluorescent
306 microscopy revealed that while PPT-GFP signal overlapped strongly with ATP5a, $PPT_{\Delta 1\text{-}13}$-

307 GFP exhibited diffuse localization throughout the nucleus and cytoplasm (Figure 5A).
308 Moreover, $PPT_{\Delta 1\text{-}36}$-GFP exhibited weak fluorescent expression mostly within the nucleus,
309 suggesting that this N-terminal truncation destabilizes PPT (Figure 5A). Pearson's correlation
310 analysis showed a strong correlation for full length PPT-GFP and ATP5a, which was
311 significantly reduced with $PPT_{\Delta 1\text{-}13}$-GFP and even more so with $PPT_{\Delta 1\text{-}36}$-GFP (Figure 5B).
312 Similarly, Mander's colocalization coefficients demonstrated that the percent of total PPT-GFP
313 overlapping with ATP5a signal was significantly reduced only in $PPT_{\Delta 1\text{-}36}$-GFP expressing
314 cells, whereas the diffuse distribution pattern of $PPT_{\Delta 1\text{-}13}$-GFP within the cell maintained strong
315 fluorescent signal overlap with ATP5a (Supplemental Figure S5A). In contrast, the total ATP5a
316 overlap with PPT-GFP was reduced for both truncation mutants (Supplemental Figure S5B).
317 Sub-cellular fractionation and Western blotting supported our microscopy results, showing
318 that while PPT-GFP and $PPT_{\Delta 1\text{-}13}$-GFP are both present in post-mitochondrial supernatant
319 (PMS) and mitochondrial fractions, $PPT_{\Delta 1\text{-}13}$-GFP accumulates in the PMS (Figure 5C),
320 suggesting difficulty in localizing to mitochondria. As expected, based on our microscopy
321 analysis, weak expression of $PPT_{\Delta 1\text{-}36}$-GFP was detected only in the PMS (Figure 5C),
322 indicating that this truncation cannot be imported into the mitochondria and appears to be less
323 stable.

324 To test whether this newfound mitochondrial localization is required for PPT to modify
325 mitochondrially localized target proteins, we transduced PPT-deficient cells with a control
326 mitochondrial DSRed (mtDSRed) construct, PPT-GFP, $PPT_{\Delta 1\text{-}13}$-GFP, or $PPT_{\Delta 1\text{-}36}$-GFP, and
327 assessed mtFAS pathway activity. Expression of PPT-GFP rescued protein lipoylation and
328 SDHB stability in PPT-deficient cells, whereas $PPT_{\Delta 1\text{-}13}$-GFP and $PPT_{\Delta 1\text{-}36}$-GFP both failed to
329 significantly increase either of these mtFAS-dependent endpoints (Figure 5D, Supplemental
330 Figure S5C). These data suggest that mitochondrial localization of PPT is required for 4'PP-
331 modification of NDUFAB1. To further investigate whether mitochondrial localization of PPT is
332 required for OXPHOS activity, we performed growth assays in glucose- and galactose-
333 containing media, with cells expressing mtDSRed, PPT-GFP, or $PPT_{\Delta 1\text{-}13}$-GFP as above, to
334 assess the ability of each construct to rescue respiration-dependent growth. Regardless of
335 rescue construct, PPT-deficient cells all still exhibited significantly reduced growth in glucose
336 media (Figure 5E, Supplemental Figure S5D). However, in galactose media, while expression
337 of PPT-GFP and $PPT_{\Delta 1\text{-}13}$-GFP both partially rescued growth of PPT-deficient cells, $PPT_{\Delta 1\text{-}13}$-
338 GFP rescued less well than the full length PPT-GFP construct (Figure 5F, Supplemental
339 Figure S5D). Together, these data demonstrate that mitochondrial localization of PPT is

340 necessary for phosphopantetheinylation of NDUFAB1, mtFAS pathway activity, and cellular
341 respiration.
342
343 **Identification of AASDHPPT patient variants of unknown significance**
344 We recently described a pathogenic variant in the mtFAS gene *MCAT* c.812T>C; p.T271I
345 (rs760294168; NM_173467.4), which displayed perturbed ETC complex assembly and
346 cellular respiration[23]. As our data demonstrate that perturbed *Aasdhppt* expression results in
347 similar phenotypes in cultured mouse skeletal myoblasts, we wondered whether there may
348 be patients with pathological variants in *AASDHPPT*. We searched the ClinVar database[24]
349 and identified several missense variants of uncertain significance (VUS) in *AASDHPPT* that
350 were associated with inborn genetic diseases. We selected six of these variants for analysis:
351 c.343C>T; p.P12S (NM_015423.3), c.140G>A; pR47H (NM_015423.3), c.214G>T; pA72T
352 (NM_015423.3), c.235T>G; pW79G (NM_015423.3), c.247C>T; pR83C (NM_015423.3), and
353 c.286A>G; pK96E (NM_015423.3). The P12S variant corresponds to an alteration in the
354 putative MTS of PPT (Figure 5) whereas the other VUS correspond to alterations in the acetyl-
355 CoA binding domain[25]. We created each of these missense mutations in our full length PPT-
356 GFP construct and assessed their ability to rescue perturbed mtFAS activity in our PPT-
357 deficient cells (Figure 6A-B). Although each construct showed some rescue capability, PPT-
358 GFP R47H and PPT-GFP W79G exhibited weaker rescue effects compared to the other
359 variants (Figure 6A-B). In particular, cells expressing the PPT-GFP W79G variant showed
360 reduced protein lipoylation and SDHB, along with low levels of GFP signal compared to the
361 other variants, despite expression from the same promoter (EF-1α promoter). This suggests
362 that this variant may have reduced protein stability. These data serve to highlight the R47H
363 and W79G variants of *AASDHPPT* as potential clinical pathologic variants, with phenotypes
364 attributable to altered mtFAS activity and perturbed cellular respiration.
365
366 **Discussion**
367 Here we show for the first time that a pool of PPT localizes to the mitochondrial matrix via
368 a N-terminal MTS, and that this mitochondrial localization is required for 4'PP-modification of
369 NDUFAB1, the mitochondrial ACP. Loss of PPT results in impaired mtFAS activity, ETC
370 assembly, and mitochondrial respiration, with a concurrent increase in reductive
371 carboxylation, as seen in other models of ETC dysfunction. We further identify two clinical
372 VUS in *AASDHPPT* that fail to rescue PPT-deficient cells, which we therefore hypothesize
373 may be disease-causing variants in human patients. Our data position PPT as a critical

374 mediator of mitochondrial oxidative function, owing to its requirement for proper function of
375 the mtFAS pathway. The observation that *AASDHPPT* most closely correlated with mtFAS
376 genes in the DepMap co-dependency dataset (Figure 2A,B, Supplemental Figure S2D,E)
377 supports the idea that activation of mtFAS, through 4'-PP modification of NDUFAB1, is the
378 essential function of PPT, followed closely by 4'-PP modification of FASN. Importantly, our
379 findings identify several fundamental unknowns: What factors regulate PPT activity, and how
380 might the sub-cellular compartment affect regulation? What process(es) control PPT targeting
381 to the mitochondria versus other compartments? How might we target the mitochondrial
382 functions of PPT in patients with disease-causing *AASDHPPT* variants?

383 The discovery of distinct pools of PPT raises questions about what factors control PPT
384 activity in each compartment. As an enzyme, PPT activity could be controlled via PTMs,
385 protein-protein interactions, or substrate availability, all of which are likely to differ between
386 the cytoplasm and mitochondria. For instance, PPT uses CoA as the substrate for 4'PP-
387 modification of target proteins. CoA abundance is drastically different between the cytoplasm
388 and mitochondria; mitochondrial free CoA is thought to be in the range of 2.55–3.35mM,
389 whereas cytoplasmic concentrations range from 50–90μM[26]. How CoA synthesis is controlled
390 and directed to various subcellular compartments is an area of active study. The first step in
391 CoA synthesis is both compartmentalized and highly regulated by pantothenate kinases
392 (PANKs), which have been proposed to act as metabolic sensors that coordinate CoA
393 synthesis and availability with the metabolic needs of the cell[26]. However, the localization of
394 some enzymatic steps further down the synthesis pathway remain unknown. Moreover, CoA
395 is transported into mitochondria via the solute carrier (SLC) protein SLC25A42, and perhaps
396 also via SLC25A16, the Graves' disease carrier protein[26], thus alterations to CoA transport
397 are another potential mechanism that could affect CoA availability in mitochondria. The effect
398 of perturbations in CoA availability on PPT enzymatic activity remains unclear, but may have
399 important implications for PPT targets such as mtFAS in diseases with CoA dysregulation
400 (synthesis defects, transport defects).

401 Beyond substrate-level regulation, PPT activity may also be controlled via regulation of its
402 own localization to the cytoplasm or mitochondria. Our data demonstrate that PPT is targeted
403 to mitochondria via a N-terminal MTS, but how this localization is controlled in cells to produce
404 two distinct pools is completely unstudied. We hypothesize several possibilities that may affect
405 the outcome of where PPT is localized: 1) at the level of transcription, via an alternate start
406 site that would exclude the MTS, 2) at the level of mRNA processing, via an alternatively
407 spliced isoform that would remove the MTS, or 3) via a post-translational modification or

408 association that would preclude the function of the MTS. Irrespective of which of these
409 mechanisms is involved, it is plausible that the choice of PPT localization may be dynamic
410 and influenced by changes in cellular state, such as differentiation or metabolic status. We
411 also unexpectedly observed a pool of PPT within the nucleus. None of the known 4'PP-
412 modified proteins are nuclear, raising the exciting possibility that PPT may have an
413 undescribed nuclear function. Future work aimed at understanding the nuclear function(s) of
414 PPT and their regulation will be crucial to developing a full understanding of PPT function in
415 cells.

416 Of note, we identified two potentially pathogenic patient variants in *AASDHPPT*. Our
417 results predict that patients harboring these mutant alleles may exhibit impaired mtFAS,
418 leading to diminished mitochondrial function. These data add to the growing list of patients
419 with mutations in mtFAS genes and other CoA metabolism genes, such as the PANKs, and
420 support the notion that impairments in CoA metabolism may cause disease via mtFAS
421 dysfunction[27,28]. Importantly, we evaluated the functionality of each variant in this study by
422 testing their ability to rescue mtFAS impairment in PPT-deficient cells. As described above, to
423 do so we ectopically expressed the missense mutation construct under the control of the
424 constitutively expressed EF-1α promoter, a strategy that we have successfully employed in
425 the past to identify a functionally impaired variant of the mtFAS gene MCAT[23]. However,
426 because this strategy relies on overexpression, it is possible that variants that cause weak
427 impairments would be able to rescue fully in this assay, because of the high levels of
428 expression. Thus, our data do not rule out the possibility that the VUS tested herein might still
429 cause mtFAS defects in endogenous settings.

430 Altogether, this study identifies AASDHPPT as the PPTase responsible for the addition of
431 4'-PP to NDUFAB1, and further demonstrates that mitochondrial localization of PPT is
432 required for this function. Future studies are needed to illuminate the processes that regulate
433 PPT activity and sub-cellular localization. Such work will be critical in improving our
434 understanding of how this pleiotropic enzyme controls mitochondrial oxidative function.

435

436 **Methods**

437

438 ***Aasdhppt mutant cell lines, growth assays, and viral transduction***

439 C2C12 immortalized mouse skeletal myoblasts (ATCC CRL-1772, verification provided by
440 ATCC) were grown in DMEM supplemented with 4.5 g/L glucose, glutamine, and sodium
441 pyruvate (Corning, 10-013-CV) and 10% FBS (Sigma, F0926) in humidified tissue culture

442 incubators at 37°C, 5% CO_2. To generate *Aasdhppt* mutant clones, four sgRNA sequences
443 (**Table 1)** were designed targeting exon 1 or exon 2 of the mouse *Aasdhppt* gene and
444 subcloned into the pLentiCRISPR v2 vector using previously described methods[29]. Parental
445 C2C12s were transfected with pLentiCRISPRv2_sgAasdhppt or empty vector. 48 hours after
446 transfection, cells were sorted on GFP signal intensity and plated into 96-well plates to obtain
447 single cell colonies for expansion and establishment of stable, clonal cell lines. Clones were
448 screened for AASDHPPT protein expression levels and two control clones and two *Aasdhppt*
449 mutant clones were selected for further experiments. For growth assays 10,000 cells/well
450 were plated in 12-well plates or 1,000 cells/well in 48-well plates and grown in DMEM with
451 either no sodium pyruvate, 4 mM glutamine, and 25 mM glucose or no sodium pyruvate, 4
452 mM glutamine, and 10 mM galactose for 3 days in technical triplicates. Tissue culture plates
453 were placed in an IncuCyte® chamber (Sartorius) and percent confluency was measured from
454 sixteen, 10X magnification fields per well for 12-well plates, or nine, 10X magnification fields
455 for 48-well plates every 6 hours. For rescue experiments, control and *Aasdhppt* mutant clonal
456 lines were transiently infected with retrovirus harboring a control transfer plasmid expressing
457 mtDSRed (pQXCIP mtDSRed) or pMMLV retrovirus vectors custom designed, synthesized,
458 and purchased from VectorBuilder (Chicago, IL, USA), harboring full length, or N-terminal
459 truncations of residues 1-13 or 1-36, of AASDHPPT with C-terminal GFP and Flag tag- fusion.
460 For generation of retrovirus constructs harboring single point mutations in the full length
461 AASDHPPT-GFP-Flag construct, primers in **Table 2** were used with a New England Biolabs
462 Q5 Site-Directed Mutagenesis Kit. Plasmid reactions were transformed into competent *E. coli*
463 and selected colonies were sequence validated for successful incorporation of point
464 mutations.
465
466 ***Genomic Sequence Analysis of AASDHPPT Mutants***
467 Approximately five million cells of each clonal mutant cell line, PPT-1 and PPT-2, were
468 pelleted and washed with PBS then frozen at -80ºC. Genomic DNA was extracted using a
469 column-based kit assay (Qiagen 69504). Aasdhppt was amplified using primers described in
470 **Table 3**, and sanger sequenced using the forward primer. Sanger sequencing peaks were
471 deconvoluted using the Indigo web-based software (https://www.gear-genomics.com)[30].
472
473 ***SDS-PAGE and immunoblotting***
474 Cultured cells were scraped from tissue culture plates directly into RIPA buffer
475 supplemented with mammalian protease inhibitor cocktail (mPIC, Millipore Sigma) and Pierce

476 Universal Nuclease, incubated at 4°C with constant agitation on a microcentrifuge tube orbital
477 shaker, then centrifuged at 17,000 x g for 20 minutes at 4°C to remove insoluble material.
478 Supernatant was then transferred to a new microcentrifuge tube to be saved as whole cell
479 lysate (WCL). For denoted protein analysis, WCL, PMS, and/or crude mitochondrial fractions
480 were first normalized for total protein content via Pierce BCA Protein assay (Thermo Fisher
481 Scientifc 23225). Samples were resolved by SDS-PAGE and transferred to nitrocellulose
482 membranes. Immunoblotting was performed using the indicated primary antibodies (**Table 4**)
483 with visualization and analysis of protein signal using Rabbit and Mouse IgG Antibody DyLight
484 680, or 800, Conjugated secondary antibodies and Bio-Rad ChemiDoc Imaging System.
485
486 ***Seahorse Extracellular Flux Rate Assay***
487 Extracellular flux rate assays were performed on a Seahorse XFe96 Analyzer (Agilent).
488 Cells from the indicated clones were plated in approximately 22 wells of a 96-well seahorse
489 plate at a density of 10,000 cells/well in DMEM +10% FBS and allowed to adhere overnight.
490 The morning of the assay, cells were washed twice and media was replaced with non-buffered
491 seahorse media (Agilent 103680) supplemented with 25 mM glucose, 2 mM glutamine, and 1
492 mM sodium pyruvate. A standard mitochondrial stress test was then performed using 1 µM
493 oligomycin, 3 µM FCCP, and 0.5 µM Rotenone + 0.5 µM Antimycin A. Baseline oxygen
494 consumption was measured three times, followed by acute injection of oligomycin, followed
495 by FCCP and finally Rotenone + Antimycin A. Measurements were standard, with acute
496 injection of drug followed by 3 minutes of mixing then measurements of oxygen levels over 3
497 minutes, with three measurements per phase. Data were normalized with crystal violet
498 absorption for approximation of cell number. Results were analyzed in WAVE software.
499
500 ***Crude mitochondrial isolation***
501 Cells were harvested and processed as previously described[13]. Briefly, cells were
502 harvested by trypsinization, washed once with cold, sterile PBS (Gibco, 10010-023), then
503 stored at -80°C. At the time of mitochondrial isolation, cell pellets were thawed and
504 resuspended in 1 mL CP-1 buffer (100 mM KCl, 50 mM Tris-HCL, 2 mM EGTA, pH 7.4)
505 supplemented with mammalian protease inhibitor cocktail (mPIC, Millipore Sigma P8340) and
506 mechanically lysed by 10 passes through a 1 mL insulin syringe with 26-guage needle and
507 centrifuged at 700 x g for 10 minutes to pellet unlysed cells and debris. Supernatant was
508 transferred to a new microcentrifuge tube and centrifuged at 10,000 x g for 10 minutes to
509 pellet the crude mitochondrial fraction. Post-mitochondrial supernatant (PMS) was used for

510 Western blot analysis or discarded. Mitochondrial pellets were resuspended in a small volume
511 of either RIPA buffer (10 mM Tris-HCl, pH 8.0, 1 mM EDTA, 0.5 mM EGTA, 1% Triton X-100,
512 0.1% Sodium Deoxycholate, 0.1% SDS, 140 mM NaCl) supplemented with mPIC, or CP-1
513 buffer, equal to approximately twice the pellet volume. Resuspended pellets were then used
514 for applications described below.
515
516 ***Blue Native-PAGE***
517 Crude mitochondrial fractions were prepared and normalized for total protein content as
518 previously described. 100 µg of mitochondria were pelleted at 10,000 x g for 10 minutes at
519 4°C. Supernatant was removed and pellets were resuspended in 60 µL of 1x pink lysis buffer
520 (Invitrogen BN2003). Digitonin (GoldBio D-180-2.5) was added to samples at a final
521 concentration of 1% mass/volume and samples were incubated on ice for 15 min. Insoluble
522 material was pelleted by centrifugation at 17,000 x g for 20 minutes and supernatant was
523 transferred to new microcentrifuge tubes. 6 µL of NativePAGE sample buffer (Invitrogen
524 BN2004) was added to samples and 10 µL of sample (~15 µg of crude mitochondrial fraction)
525 was loaded per lane on pre-cast 3-12%, Bis-Tris NativePAGE gels (Invitrogen BN1001BOX)
526 with NativePAGE anode buffer (Invitrogen 2001) and dark blue cathode buffer (Invitrogen
527 BN2002) at 150V for 30-40 minutes then switched to light blue cathode buffer and run at 20
528 V overnight. Gels were then transferred to PVDF membranes at 100 V for 2 hours and blotted
529 with the indicated primary antibodies (**Table 4**. Secondary anti-mouse HRP antibody and
530 SuperSignal West Femto Maximum Sensitivity Substrate (Thermo Fisher Scientific 34096)
531 was used to visualize bands with a Bio-Rad ChemiDoc Imaging System.
532
533 ***Glutamine Tracing***
534 The indicated clonal cell lines were plated in 6-well plates in triplicate at a density of 200K
535 for PPT-1 and PPT-2, and 175K for Ctrl-1 and Ctrl-2 to account for differences in growth rate.
536 Cells were allowed to adhere for two hours, at which point the media was changed to
537 unlabeled media (Corning DMEM 17-207-CV with 1mM sodium pyruvate, 5mM glucose, and
538 4mM glutamine). After twenty hours in unlabeled media, wells were changed to labeled media
539 at the indicated time points prior to harvest (Corning DMEM 17-207-CV with 1mM sodium
540 pyruvate, 5mM glucose, and 4mM $U^{13}C$-glutamine). Three wells per cell line were left
541 unlabeled for natural isotope abundance correction, and another three per cell line were used
542 to determine cell number at the time of freezing. 24 hours after cells were in unlabeled media,
543 all wells were washed with normal saline once and frozen at -80°C. Plates were then extracted

544 for metabolites using a volume of 40:20:20 methanol:acetonitrile:water scaled to the number
545 of cells determined by the cell count wells (average from three wells). Lysates were sonicated
546 and incubated on ice for 60 minutes. At this point any insoluble material was spun out of the
547 sample at 17,000 x g for 10 minutes at 4°C. 1000 µL of supernatant was dried using a
548 SpeedVac concentrator. Dried metabolomics extracts were next resuspended in 100% water
549 containing 25 µg/mL D5-Glutamate (DLM-556, Cambridge) such that resuspension sample
550 equivalents were 5.82E+3 cells/µL. 2 µL of resuspended samples were injected on column, a
551 process blank was analyzed before and after experimental samples, and a pooled sample
552 was injected twice before experimental samples for column conditioning, and every 7-10
553 sample injections thereafter. Data dependent MS2 (ddMS2) data was collected from pooled
554 experimental replicates to identify group-specific compounds.

555 Data were collected on a Vanquish liquid chromatography system coupled to an Orbitrap
556 Exploris 240 (Thermo Fisher Scientific) using a heated electrospray ionization (H-ESI) source
557 in ESI negative mode. All samples were run through a 24-minute reversed-phase
558 chromatography ZORBAX extend-C18 column (1.8 µm, 2.1mm × 150mm, 759700-902,
559 Agilent, California, USA) combined with a guard column (1.8 µm, 2.1 mm × 5 mm, 821725-
560 907, Agilent). Mobile phase A was LC/MS H2O (W6-4, Fisher) with 3% LC/MS grade MeOH
561 (A456-4, Fisher), mobile phase B was LC/MS grade methanol (A456-4, Fisher), and both
562 mobile phases contained 10 mM tributylamine (90780-100ML, Sigma), 15 mM acetic acid,
563 and 0.01% medronic acid (v/v, 5191-4506, Agilent). For the re-equilibration gradient, mobile
564 phase A was kept the same, and mobile phase B was 99% LC/MS grade acetonitrile (A955-
565 4, Fisher). Column temperature was kept at 35ºC, flow rate 0.25 mL/min, and the solvent
566 gradient was as follows: 0-2.5 min held at 0% B, 2.5-7.5 min from 0% B to 20% B, 7.5-13 min
567 from 20% B to 45% B, 13-20 min from 45% B to 99% B, and 20-24 min held at 99% B. The
568 analytical solvent gradient was followed by a 16 min re-equilibration gradient to prep the
569 column before the next sample injection that went as follows: 0-0.05 min held at 99% B at
570 0.25 mL/min, 0.05-1 min from 99% B to 50% B and 0.25 mL/min to 0.1 mL/min, 1-11 min held
571 at 50% B and 0.1 mL/min, 11-11.05 min from 50% B to 0% B at 0.1 mL/min, 11.05-14 min held
572 at 0% B at 0.1 mL/min, 14-14.05 min held at 0% B and increased flow rate from 0.1 mL/min
573 to 0.25 mL/min, and 14.05-16 min held at 0% B and 0.25 mL/min. The mass spectrometer
574 acquisition settings were as follows: source voltage -2,500V, sheath gas 60, aux gas 19,
575 sweep gas 1, ion transfer tube temperature 320ºC, and vaporizer temperature 250ºC. Full
576 scan data were collected with a scan range of 70-800 m/z at a mass resolution of 240,000.
577 Fragmentation data was collected using a data-dependent MS2 (ddMS2) acquisition method

578 with MS1 mass resolution at 120,000, MS2 mass resolution at 15,000, and HCD collision
579 energy fixed at 30%.
580 Natural isotope abundance correction was done using the FluxFix Isotopologue Analysis
581 Tool*14* (version 0.1) web-based application[31]. Data analysis was conducted in Skyline (version
582 23.1.0.268), consisting of peak picking and integration, using an in-house curated compound
583 database of accurate mass MS1 and retention time derived from analytical standards and/or
584 MS2 spectral matches for the specified chromatography method.
585
586 ***AASDHPPT co-essentiality analysis and network modeling***
587 Gene essentiality scores and gene co-dependency Pearson correlation values were
588 obtained from the DepMap Portal Project Achilles 23Q4 release[17,32–34] in which genome-wide
589 CRISPR loss-of-function screens were performed in 1100 human cancer cell lines. Co-
590 Dependency plots between AASDHPPT and other genes were generated from gene
591 essentiality scores for each cancer line obtained directly from the DepMap Portal. For two-
592 dimensional network analysis, gene essentiality correlations for a custom list of genes were
593 used to create a data matrix (see Supplementary Excel File**)**. From this matrix, methodologies
594 and code originally published by Arnold et al.[35] and available at: https://github.com/finley-
595 lab/coessentiality-network were first used to generate a correlation matrix heatmap of
596 codependent gene modules. Co-dependent gene modules were then visualized as a network
597 diagram and genes with low correlation scores (Pearson $r < 0.2$) were filtered out as previously
598 described[35]. Graph edges were weighted according to the strength of pairwise gene
599 correlations.
600
601 ***Cell immunostaining and microscopy analysis***
602 Denoted C2C12 cell lines were seeded into chambered cover glass slides and cultured
603 overnight. The following day, cells were fixed in ice-cold 4% paraformaldehyde (PFA) in PBS
604 solution for 10 minutes at room temperature, followed by 3 washes in 1X PBS solution. Cells
605 were then permeabilized and blocked in PBS solution containing 0.5% BSA, 5% goat serum,
606 and 0.3% Triton X-100 for 1 hour at room temperature. Cells permeabilized/blocked with
607 blocking buffer were then incubated with denoted primary antibodies overnight at 4°C followed
608 by washes with 1X PBS prior to incubation with Alexa Fluor conjugated secondary antibodies
609 (**Table 4**) for 2 hours at room temperature. Washes were repeated and cells were then stained
610 with Hoechst Dye for 10 minutes at room temperature. After subsequent washes, samples

611 were then imaged on a Zeiss LSM 880 with Airyscan and non-linear optics microscope, using
612 a 40X water objective and 1.2 NA to collect z-stacks.
613 For quantification of endogenous AASDHPPT expression in control and *Aasdhppt* mutant
614 clonal lines, regions of interest (ROIs) were manually drawn with Fiji software for individual
615 cells from channels with fluorescent ATP5a expression. Area was then measured for each
616 ROI with corresponding mean fluorescent intensity of signal from the AASDHPPT fluorescent
617 channel. Mean fluorescent intensity per cell area was then calculated.
618 For colocalization analysis of endogenous AASDHPPT or AASDHPPT-GFP fusion
619 constructs with mitochondrial proteins in maximum intensity projections of each imaged field,
620 nuclear signal detected by Hoechst Dye staining was first used to create ROIs in Fiji. Pixels
621 with signal detected in nuclear ROIs in red and green channels were then removed from
622 images of the same field prior to merging of red and green channels so that colocalization
623 analysis would be exclusive of nuclei and limited to subcellular organelles and cytoplasmic
624 regions. Merged channels were then processed by the BIOP JACoP Fiji plugin
625 (https://c4science.ch/w/bioimaging_and_optics_platform_biop/image-
626 processing/imagej_tools/jacop_b/) using the Otsu method of thresholding for each channel to
627 generate Pearsons Correlation values and Manders Colocalization Coefficients.
628
629 ***Sub-mitochondrial Localization Assay***
630 The crude mitochondrial fraction and post-mitochondrial supernatant (PMS) fractions were
631 isolated as described above from C2C12 cells expressing C' GFP-tagged AASDHPPT via a
632 EF-1α promoter. The crude mitochondrial fraction was washed with CP-1 buffer without mPIC
633 twice, and resuspended at a concentration of 5µg/µL, as determined by BCA assay. A total of
634 25 µg was then diluted to 100 µL with CP-1 buffer with or without 2 µg/mL proteinase K (New
635 England Biolabs P8107S) and the indicated concentration of digitonin or 2% Triton. Samples
636 were incubated on ice for 30 minutes, then the proteinase activity was halted with the addition
637 of mPIC, and the remaining crude mitochondria pelleted at 12,500 x g for 5 minutes at 4°C.
638 Pellets were then resuspended in 50uL Laemli buffer, and samples were resolved on SDS-
639 PAGE 4-20% gradient gels (BioRad 4561094). Proteins were transferred to nitrocellulose
640 membranes and immunoblotted for the GFP tag and for proteins of known mitochondrial
641 localization using the indicated primary antibodies (**Table 4**)
642
643 ***Bimolecular fluorescence complementation (BiFC) assay***

644 To generate BiFC cell lines, five split-Venus constructs were designed and synthesized by
645 VectorBuilder in a pMMLV retroviral backbone. Constructs were designed to contain either the
646 C' terminal half of the Venus tag with blasticidin resistance (VC), or the N' terminal half of the
647 Venus tag with puromycin resistance (VN). VC constructs were tagged to the C' terminal end
648 of *citrate synthase* (CS-VC), *mitofusin 2* (MFN2-VC) or *Ndufab1* (NDUFAB1-VC). VN
649 constructs were tagged to either the C' or N' terminal end of *Aasdhppt* (PPT-VN and VN-PPT,
650 respectively). Following retroviral packaging in HEK293T cells, 40,000 wildtype C2C12 cells
651 were transduced to express either PPT-VN or VN-PPT in combination with each VC construct.
652 Negative control lines were generated by transducing cells with individual VC or VN constructs
653 alongside an empty vector control (PQXCIP for VC constructs, and PQXCIB for VN
654 constructs). This ensured that all cells were transduced with an approximately equal total viral
655 load. Stable populations were derived via combined puromycin and blasticidin selection (2
656 µg/mL each), yielding 11 cell lines in total; 6 with combined VC/VN constructs plus 5 single
657 construct controls.
658 For measurement of fluorescence, approximately 100,000 cells were trypsinized and
659 resuspended in 200 µL PBS. Cell suspensions were then assessment on an Accuri bench-top
660 cytometer, recording a minimum of 20,000 events per sample. The percentage of Venus-
661 positive cells was analyzed using FlowJo (v. 10.10.0). Fluorescence intensity histograms were
662 generated using FlowJo Layout Editor. Visual confirmation of fluorescence achieved by
663 imaging all BiFC cell lines on a Nikon Eclipse Ti2 microscope. Briefly, 20,000 cells per cell line
664 were seeded in chamber cover slides (Cellvis, C4-1.5H-N). After 24 hours, cells were fixed in
665 4% PFA for 30 mins at room temperature before imaging the following day (20X objective,
666 0.75 NA).
667
668 ***Statistical analysis***
669 Statistical analysis was performed using GraphPad Prism 10. Unless otherwise note, data
670 were analyzed by one-way ANOVA followed by Dunnett's multiple comparison test (when
671 compared to only control) or Šídák's or Tukey's multiple comparison test (when comparing all
672 groups). A p-value of <0.05 was considered statistically significant. Data that included a third
673 vairable (ex. time) was analyzed by two-way ANOVA followed by Tukeys multiple comparison
674 test.
675
676 **Table 1**

sgRNA cloned into pLentiCRISPRv2	sequence

PPT 1	GATGCGGTCTATCCAGCCGG
PPT 2	GCAGACGGATATGATCCCAA
PPT 3	AGCGGACCGAGCCGGTCGTA
PPT 4	GGAACACCATACGACCGGCT

677

678 **Table 2**

Primers for site-directed mutagenesis	**sequence**
P12S Fwd	GTGCGTGGTGAGCTCCATGGAGG
P12S Rev	AGCCTCTTAGCGGGG
R47H Fwd	GGAGAAGGAGCATATCGGCAAGTTC
R47H Rev	TCCGGCTGGATAGAC
A72T Fwd	GAAATTAGTTACCGAGAAATTGAATATCCC
A72T Rev	CTTATCATCAAACGACCAG
W79G Fwd	GAATATCCCTGGCGATCATATCCGTC
W79G Rev	AATTTCTCTGCAACTAATTTC
R83C Fwd	GGATCATATCTGCCTGCAGAGAAC
R83C Rev	CAAGGGATATTCAATTTCTC
K96E Fwd	GGTTCTTGCGGAAGACTCGTTGA
K96E Rev	GGCTTTCCCTTTGAAGTTCTC

679

680 **Table 3**

681

Primers for Genomic Amplification of *Aasdhppt*	
Forward Primer	TACCTGGCTTGAGGATCAGC
Reverse Primer	GGTTCTGCAGCAAGAACTGCAT

682

683

684 **Table 4**

Antibodies	**Source and reference number**
AASDHPPT	Proteintech 11244-1-AP
β-actin	Proteintech 66009-1-Ig
GRIM19	Abcam ab110240

SDHA	Abcam ab14715
UQCRFS1	Abcam ab14746
MTCO1	Abcam ab110270
ATP5a	Abcam ab14748
Lipoic acid	Millipore 437695
SDHB	Abcam ab14714
Mfn2	Cell Signaling Technologies 9482S
Citrate Synthase	Cell Signaling Technologies 14309S
NDUFAB1	Abcam ab96230
GFP	Abcam ab290
Goat anti-Mouse IgG (H+L) AlexaFluor 568	Thermo Fisher A-11004

Acknowledgments

This work was supported by funding from the NIH (R35GM151245 to SMN) and the Van Andel Institute – Metabolism & Nutrition (MeNu) Program. We thank the Meijer Foundation for financial support of MC and EM. We also thank the Van Andel Institute's Flow Cytometry Core (RRID:SCR_022685) for their assistance with single cell sorting for generation of clonal cell lines, the Metabolomics and Mass Spectrometry Core (RRID:SCR_024903) for their assistance with labeled glutamine tracing experiments and analysis, the Optical Imaging Core (RRID:SCR_021968) for their assistance with airyscan microscopy, and the Bioinformatics and Biostatistics Core (RRID:SCR_024762) for their assistance with gene essentiality score correlation network analysis.

Figure Legends

Figure 1. AASDHPPT is required for mitochondrial oxidative metabolism.
(A) Whole cell lysates were immunoblotted for the denoted targets. Data are representative of three biological replicates (B-C) Cells were grown in either 25 mM glucose (B) or 10 mM galactose (C) in an IncuCyte® system with images captured every 6 hours for 3 days. Data represent the mean confluency; error bars denote SEM * = $p < 0.05$. ns = no significance. (D) Seahorse mitochondrial stress test for Oxygen Consumption Rate (OCR). (E) Blue-native PAGE separation of isolated mitochondrial protein complexes from denoted cell lines, followed

708 by immunoblot with the indicated antibodies. Data are representative of three biological
709 replicates. (F) Schematic of isotopomeric labeling patterns upon substitution of $U^{13}C$-
710 glutamine for unlabeled glutamine. Open circles indicate ^{12}C carbons, where circles with grey,
711 red, or blue, indicate ^{13}C carbons. (G-H) Triplicate samples of the indicated cell lines cultured
712 in $U^{13}C$-glutamine for the indicated time points, harvested, and analyzed via LC-MS. Steady
713 state metabolite pool sizes and ratios are shown for the 4-hour labeling time point. (I-K)
714 Fractional enrichment of given isotopologues is represented as percentage of the total pool
715 at each indicated time point. Ratio of Citrate M+5 to Citrate M+4 and statistical comparisons
716 are shown for the four-hour time point. Error bars represent SEM (B, C), SD (D, G, H, J). * =
717 $p<0.05$ ** = $p<0.01$, *** = $p<0.001$, **** = $p<0.0001$ as determined by one-way ANOVA (G, H,
718 J) or two-way ANOVA (I, K) and Tukey multiple comparisons test
719
720 **Figure 2. AASDHPPT is required for mitochondrial fatty acid synthesis pathway**
721 **function.**
722 (A-D) Codependency plots of gene essentiality scores comparing *AASDHPPT* with
723 *NDUFAB1* (A), *ALDH1L2* (B), *DHRS2* (C), and *OXSM* (D) from DepMap CRISPR screens[17,32–
724 34,36]. (E) Two-dimensional network diagram representing gene essentiality score correlations
725 between selected genes associated with *AASDHPPT* and known substrate targets, mtFAS
726 pathway members, LYRM family members, and the GO term “pantothenate metabolism” using
727 a minimum threshold correlation score > 0.2. Different colors represent genes associated with
728 clusters as shown in Supplemental Figure 2F. Correlation strength is represented by the length
729 and thickness of the connecting edge. (F) Whole cell lysates immunoblotted for the denoted
730 targets. Data are representative of three biological replicates. # denotes non-specific bands.
731 Red asterisk denotes positive PPT expression band in clonal controls that is reduced in PPT-
732 deficient mutants. (G) Whole cell lysates from indicated cell lines expressing either mtDSRed
733 or PPT-GFP fusion protein were immunoblotted for protein expression of the denoted targets.
734 Data are representative of three biological replicates. (H) Seahorse standard mitochondrial
735 stress test to determine Oxygen Consumption Rate (OCR). Data are representative of three
736 independent experiments. Error bars represent SD.
737
738 **Figure 3. A portion of AASDHPPT localizes to mitochondria.**
739 (A) Representative 40X HPF images of *Aasdhppt* mutants and control clonal cell lines
740 immunostained with Hoechst dye to visualize nuclei and antibodies against AASDHPPT (red)
741 and ATP5a (green). (B) Quantification of mean fluorescent intensity of AASDHPPT expression

742 per cell area (µm^2) in *Aasdhppt* mutants and control clonal cell lines as represented in (A). (C)
743 Quantification of AASDHPPT and ATP5a signal colocalization outside of the nucleus
744 assessed by Pearson's correlation coefficient in double immunostained control and *Aasdhppt*
745 mutant clonal lines as represented in (A). (D) Subcellular fractionation of *Aasdhppt* mutant cell
746 lines and control. Post-mitochondrial supernatant (PMS) and mitochondrial lysate (Mito) was
747 isolated from the denoted cell lines, normalized for total protein via BCA assay, and
748 immunoblotted for AASDHPPT, ATP5a, and GAPDH. (E) Representative 40X HPF images of
749 WT skeletal muscle myoblasts expressing AASDHPPT-GFP (PPT-GFP) immunostained with
750 Hoechst dye and antibody against ATP5a (red). Scale bars represent 100 µm. Dashed
751 outlines denote magnified regions shown in panels with solid outlines. For all statistical
752 analysis data represent the mean; error bars denote SD. **** = $p<0.0001$ as determined by
753 one-way ANOVA with Šidák's multiple comparisons test.
754
755 **Figure 4. Mitochondrial AASDHPPT is inside the mitochondrial matrix.**
756 (A) Proteinase K protection assay for sub-mitochondrial localization. Crude isolated
757 mitochondria were incubated with proteinase K and treated with increasing concentrations of
758 digitonin or Triton X-100, as indicated, then blotted for GFP to assess PPT-GFP sub-
759 mitochondrial localization by comparing with proteins with known localization. MFN2 localizes
760 to the outer mitochondrial membrane (OMM) and citrate synthase (CS) localizes to the matrix.
761 Data are representative of three biological replicates. (B) Representative histograms of Venus
762 (FITC) fluorescence in the indicated BiFC cell lines. (C) Percentage of Venus-positive cells in
763 the indicated cell lines as measured by flow cytometry. Data represent the mean; error bars
764 denote standard deviation (n = 3 per group). Statistical significance was determined by one-
765 way ANOVA with Tukey's multiple comparison test. (D) Representative 20X images of
766 endogenous Venus fluorescence in VC + VN BiFC cell lines. Scale bars represent 50 µm.
767
768 **Figure 5. Mitochondrial localization of AASDHPPT is required for mtFAS function.**
769 (A) Representative 40X HPF images of WT skeletal muscle myoblasts expressing
770 mtDSRed, PPT-GFP, 13 residue N-terminal truncation of PPT ($PPT_{\Delta 1\text{-}13}$-GFP), or 36 residue
771 N-terminal truncation of PPT ($PPT_{\Delta 1\text{-}36}$-GFP) constructs immunostained with Hoechst dye and
772 antibody against ATP5a. Scale bars represent 100 µm. Dashed outlines denote magnified
773 regions shown in panels with solid outlines. Arrows denote weak expression of GFP signal
774 detected. (B) Quantification of PPT-GFP and ATP5a signal colocalization outside of the
775 nucleus assessed by Pearson's correlation coefficient in immunostained cells as represented

776 in (A). Data represent the mean; error bars denote SD. **** = p<0.0001, ns = not significant
777 determined as by one-way ANOVA with Dunnett's multiple comparisons test. (C) Subcellular
778 fractionation of WT cells expressing PPT-GFP, $PPT_{\Delta 1\text{-}13}$-GFP, or $PPT_{\Delta 1\text{-}36}$-GFP. Post-
779 mitochondrial supernatant (PMS) and mitochondrial lysate (Mito) was isolated from the
780 denoted cell lines, normalized for total protein via BCA assay, and immunoblotted detection of
781 the indicated targets. Immunoblots are representative of three biological replicates. (D) Whole
782 cell lysates from cells expressing mtDSRed, PPT-GFP, $PPT_{\Delta 1\text{-}13}$-GFP, or $PPT_{\Delta 1\text{-}36}$-GFP were
783 immunoblotted for the denoted targets. Data are representative of n > 3 biological replicates.
784 (E and F) Cells were seeded in either 25 mM glucose or 10 mM galactose and grown in an
785 IncuCyte® system with images captured every 6 hours for 3 days. Percent confluency
786 measured by IncuCyte® software. Statistical analysis for measurements at 72 hrs was
787 performed with one-way ANOVA and Tukey's multiple comparisons test. * = p <0.05. *** = p
788 <0.001. **** = p <0.0001. Data presented are mean ± SEM from one experiment
789 representative of three biological replicates.
790
791 **Figure 6. Two variants of uncertain significance in AASDHPPT fail to rescue mtFAS**
792 **activity in PPT-deficient cells.**
793 (A and B) Whole cell lysates from clonal control and duplicate *Aasdhppt* mutant clones
794 transduced with retrovirus expressing mtDSRed, PPT-GFP P12S, PPT-GFP R47H, PPT-GFP
795 A72T, PPT-GFP W79G, PPT-GFP R83C, or PPT-GFP K96E were separated by SDS-PAGE
796 and immunoblotted for the denoted targets. Immunoblots are representative of three biological
797 replicates.
798
799 **Supplemental Figure 1. AASDHPPT is required for mitochondrial oxidative metabolism.**
800 (A) Sequence analysis of sgRNA-targeted region in clonal Aasdhppt mutant cell lines, and
801 corresponding mutations generated. (B) Representative IncuCyte® phase contrast images
802 from cells denoted in Figure 1B and C at 72 hours grown in glucose or galactose
803 supplemented DMEM. Scale bars represent 200 µm. (C-G) Pool size of the indicated
804 metabolites from steady state metabolomics analysis at the four-hour labeling time point. Error
805 bars represent SD. Significance was determined by one-way ANOVA. ** = p <0.01. *** = p
806 <0.001. **** = p <0.0001. NS = not significant.
807
808 **Supplemental Figure 2. AASDHPPT is required for mitochondrial fatty acid synthesis**
809 **pathway function.**

(A-E) Codependency plots of gene essentiality scores comparing *AASDHPPT* with *FASN* (A), *AASDH* (B), *ALDH1L1* (C), *MCAT* (D), and *MECR* (E) from DepMap CRISPR screens[17,32–34,36]**.** **(**F) Heatmap depicting hierarchical clustering of pairwise gene essentiality score correlations of PPT, known PPT substrate targets, mtFAS pathway members, LYRM family members, and genes associated with the GO term "pantothenate metabolism." (G) Two-dimensional network diagram representing gene essentiality score correlations between all genes denoted in (F), no significance cutoff filter.

Supplemental Figure 3. A portion of AASDHPPT localizes to mitochondria

(A and B) Quantification of AASDHPPT and ATP5a signal colocalization outside the nucleus assessed by Manders' colocalization coefficient in double immunostained control and *Aasdhppt* mutant clonal lines as represented in (Figure 3A). Data represent the mean; error bars denote SD. **** = p<0.0001, NS = not significant as determined by one-way ANOVA with Šidák's multiple comparisons test.

Supplemental Figure 5. Mitochondrial localization of AASDHPPT is required for mtFAS function

(A and B) Quantification of PPT-GFP and ATP5a signal colocalization outside the nucleus assessed by Manders' colocalization coefficient in immunostained cells as represented in (Figure 5A). (C) Quantification of lipyol-DLAT, lipoyl-DLST, and SDHB levels relative to β-actin from SDS-PAGE analysis as shown in Figure 5DI. (D) Representative IncuCyte® phase images from cells denoted in Figure 5E and F at 72 hours grown in glucose or galactose supplemented DMEM. Scale bars represent 200 µm.For all statistical analysis data represent the mean; error bars denote SD. * = p <0.05. ** = p <.01. **** = p<0.0001, ns = not significant as determined by one-way ANOVA with Dunnett's multiple comparisons test.

FIGURE 1

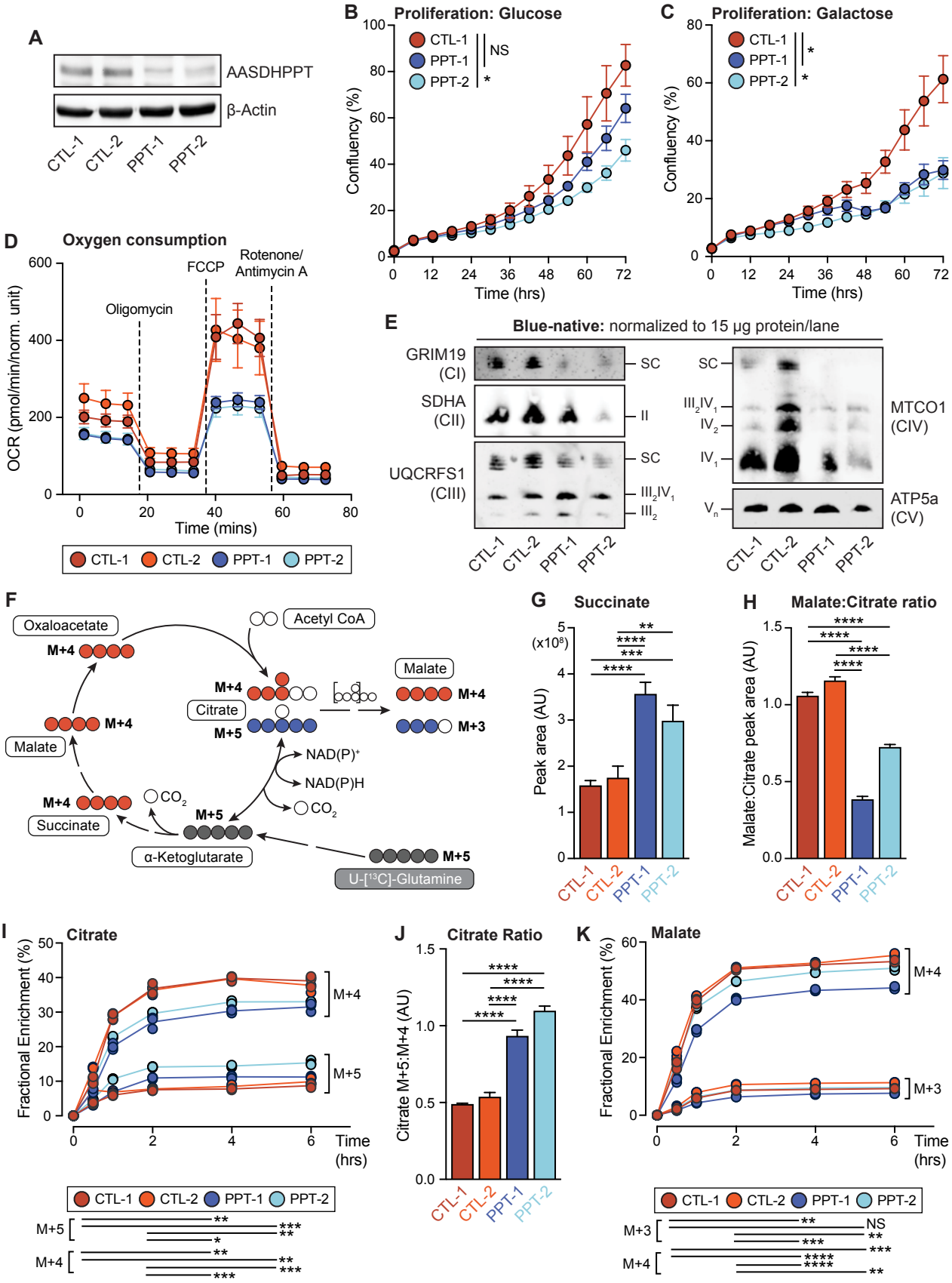
A
AASDHPPT
β-Actin
CTL-1
CTL-2
PPT-1
PPT-2
B
Proliferation: Glucose
Confluency (%)
Time (hrs)
NS
*
C
Proliferation: Galactose
D
Oxygen consumption
OCR (pmol/min/norm. unit)
Oligomycin
FCCP
Rotenone/
Antimycin A
Time (mins)
E
Blue-native: normalized to 15 µg protein/lane
GRIM19
(CI)
SDHA
(CII)
UQCRFS1
(CIII)
MTCO1
(CIV)
ATP5a
(CV)
SC
F
Oxaloacetate
Acetyl CoA
Malate
Citrate
Succinate
α-Ketoglutarate
U-[13C]-Glutamine
NAD(P)+
NAD(P)H
CO2
M+4
M+5
M+3
G
Succinate
Peak area (AU)
(x10^8)
H
Malate:Citrate ratio
Malate:Citrate peak area (AU)
I
Citrate
Fractional Enrichment (%)
Time
(hrs)
J
Citrate Ratio
Citrate M+5:M+4 (AU)
K
Malate
M+3

FIGURE 2

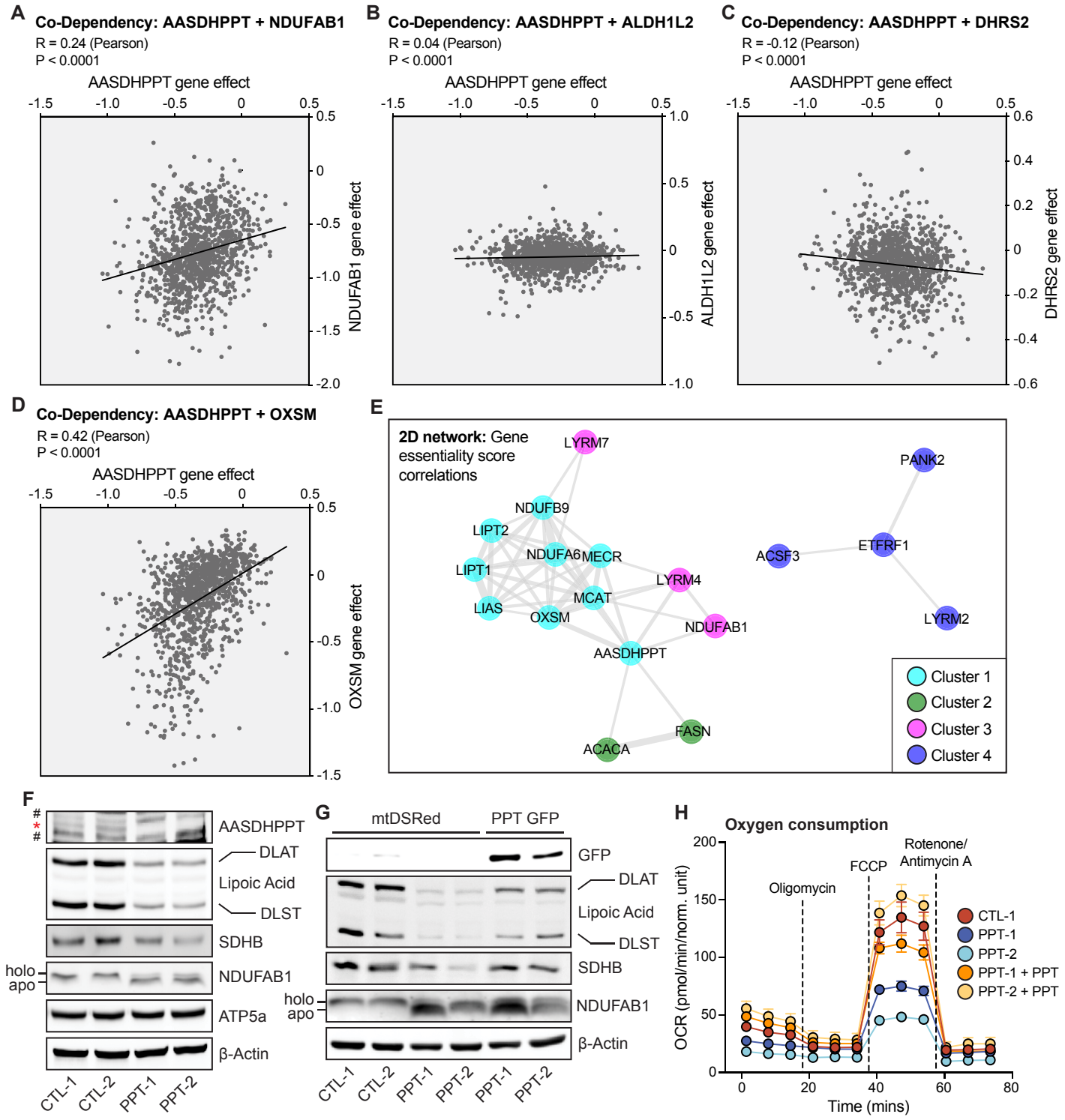
A
Co-Dependency: AASDHPPT + NDUFAB1
R = 0.24 (Pearson)
P < 0.0001
AASDHPPT gene effect
NDUFAB1 gene effect
B
Co-Dependency: AASDHPPT + ALDH1L2
R = 0.04 (Pearson)
P < 0.0001
AASDHPPT gene effect
ALDH1L2 gene effect
C
Co-Dependency: AASDHPPT + DHRS2
R = -0.12 (Pearson)
P < 0.0001
AASDHPPT gene effect
DHRS2 gene effect
D
Co-Dependency: AASDHPPT + OXSM
R = 0.42 (Pearson)
P < 0.0001
AASDHPPT gene effect
OXSM gene effect
E
2D network: Gene essentiality score correlations
LYRM7
PANK2
NDUFB9
LIPT2
NDUFA6
MECR
ACSF3
ETFRF1
LIPT1
LYRM4
MCAT
LIAS
OXSM
NDUFAB1
LYRM2
AASDHPPT
FASN
ACACA
Cluster 1
Cluster 2
Cluster 3
Cluster 4
F
AASDHPPT
DLAT
Lipoic Acid
DLST
SDHB
holo
apo
NDUFAB1
ATP5a
β-Actin
CTL-1
CTL-2
PPT-1
PPT-2
G
mtDSRed
PPT GFP
GFP
DLAT
Lipoic Acid
DLST
SDHB
holo
apo
NDUFAB1
β-Actin
CTL-1
CTL-2
PPT-1
PPT-2
PPT-1
PPT-2
H
Oxygen consumption
Oligomycin
FCCP
Rotenone/
Antimycin A
OCR (pmol/min/norm. unit)
Time (mins)
CTL-1
PPT-1
PPT-2
PPT-1 + PPT
PPT-2 + PPT

FIGURE 3

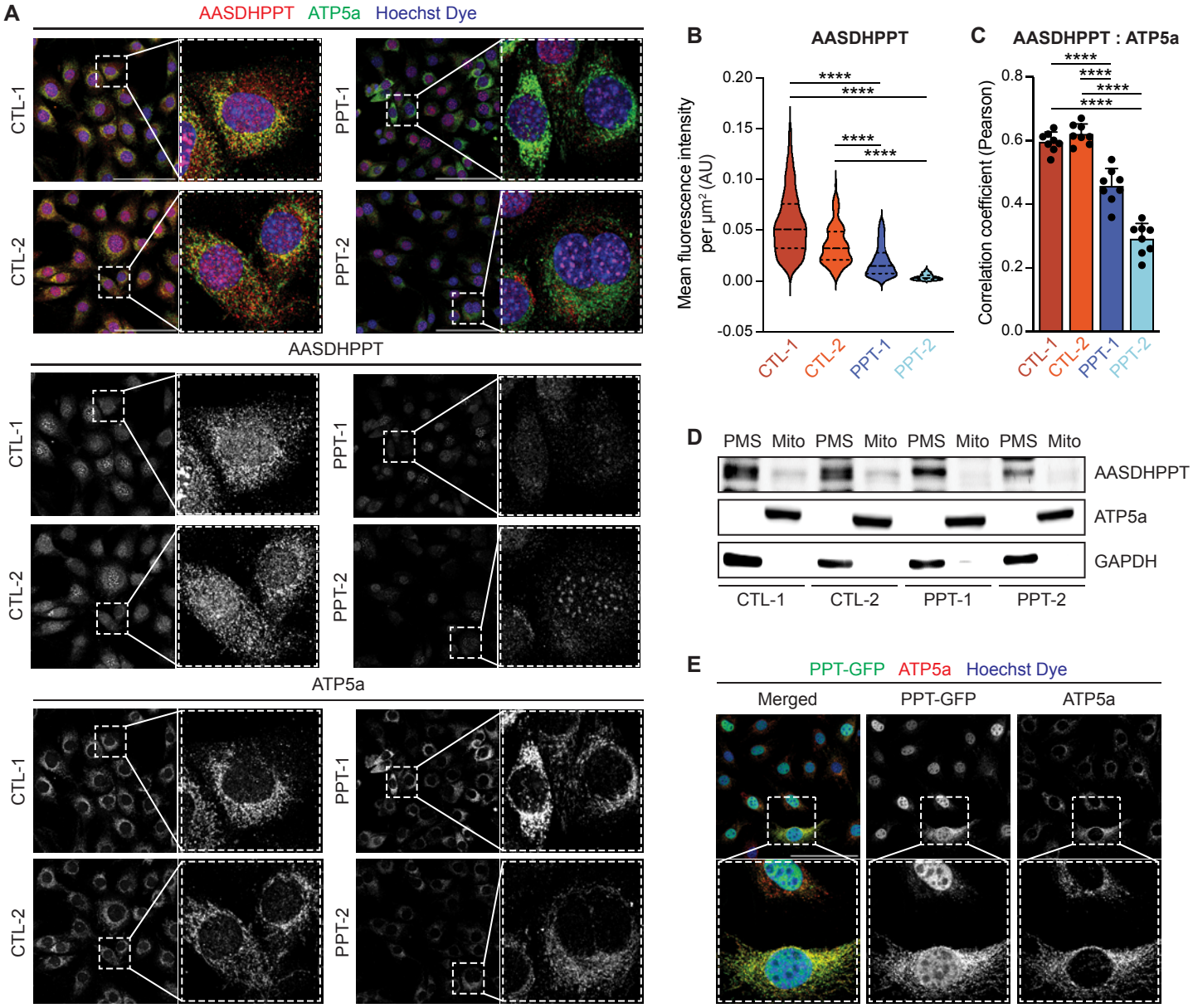
A
AASDHPPT ATP5a Hoechst Dye
CTL-1
CTL-2
PPT-1
PPT-2
AASDHPPT
ATP5a
B
AASDHPPT
Mean fluorescence intensity per µm² (AU)
0.20
0.15
0.10
0.05
0.00
-0.05
****
CTL-1
CTL-2
PPT-1
PPT-2
C
AASDHPPT : ATP5a
Correlation coefficient (Pearson)
0.8
0.6
0.4
0.2
0.0
D
PMS Mito PMS Mito PMS Mito PMS Mito
AASDHPPT
ATP5a
GAPDH
E
PPT-GFP ATP5a Hoechst Dye
Merged
PPT-GFP
ATP5a

FIGURE 4

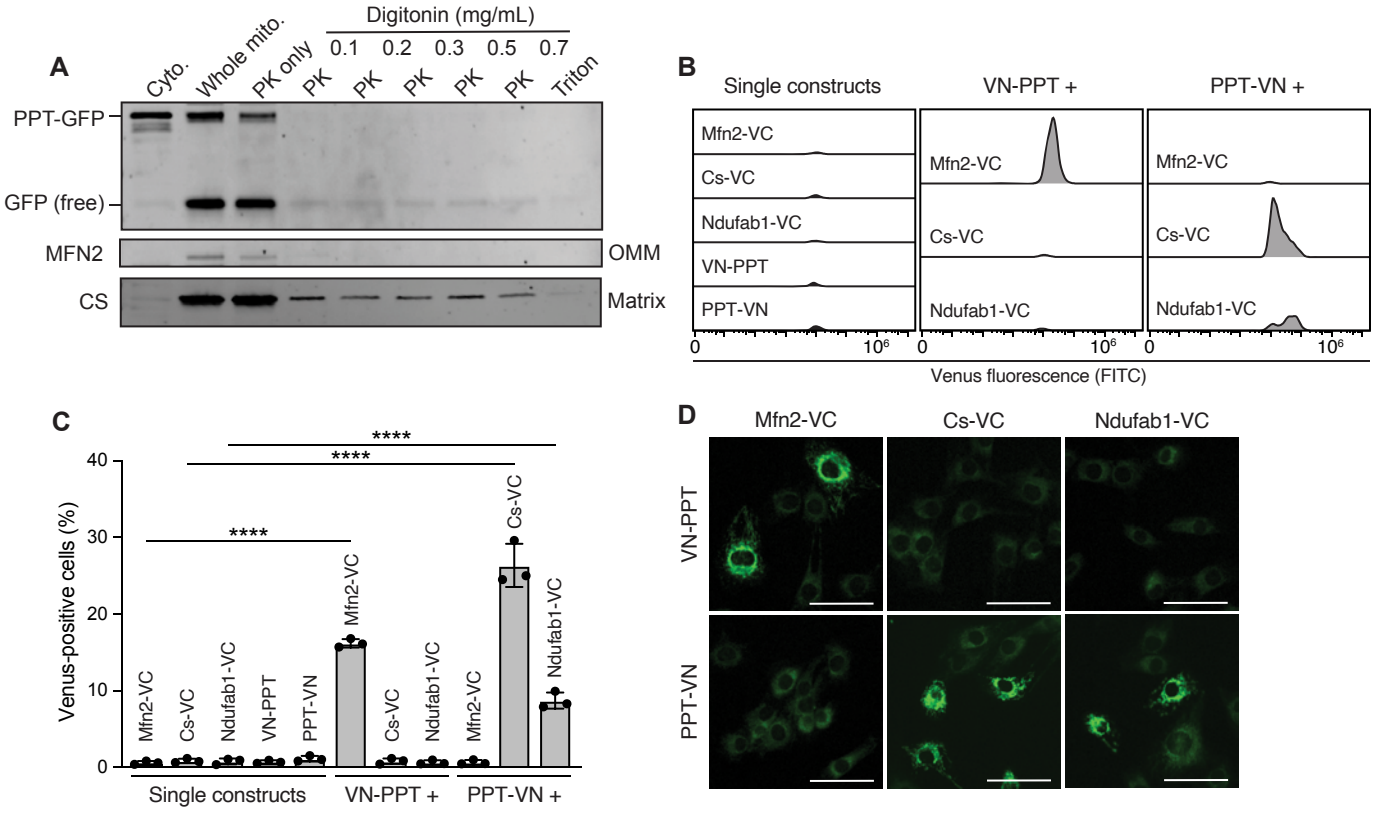
A
Cyto.
Whole mito.
PK only
Digitonin (mg/mL)
0.1
0.2
0.3
0.5
0.7
PK
Triton
PPT-GFP
GFP (free)
MFN2
OMM
CS
Matrix
B
Single constructs
VN-PPT +
PPT-VN +
Mfn2-VC
Cs-VC
Ndufab1-VC
VN-PPT
PPT-VN
0
10^6
Venus fluorescence (FITC)
C
Venus-positive cells (%)
40
30
20
10
0
****
Single constructs
VN-PPT +
PPT-VN +
D
Mfn2-VC
Cs-VC
Ndufab1-VC
VN-PPT
PPT-VN

FIGURE 5

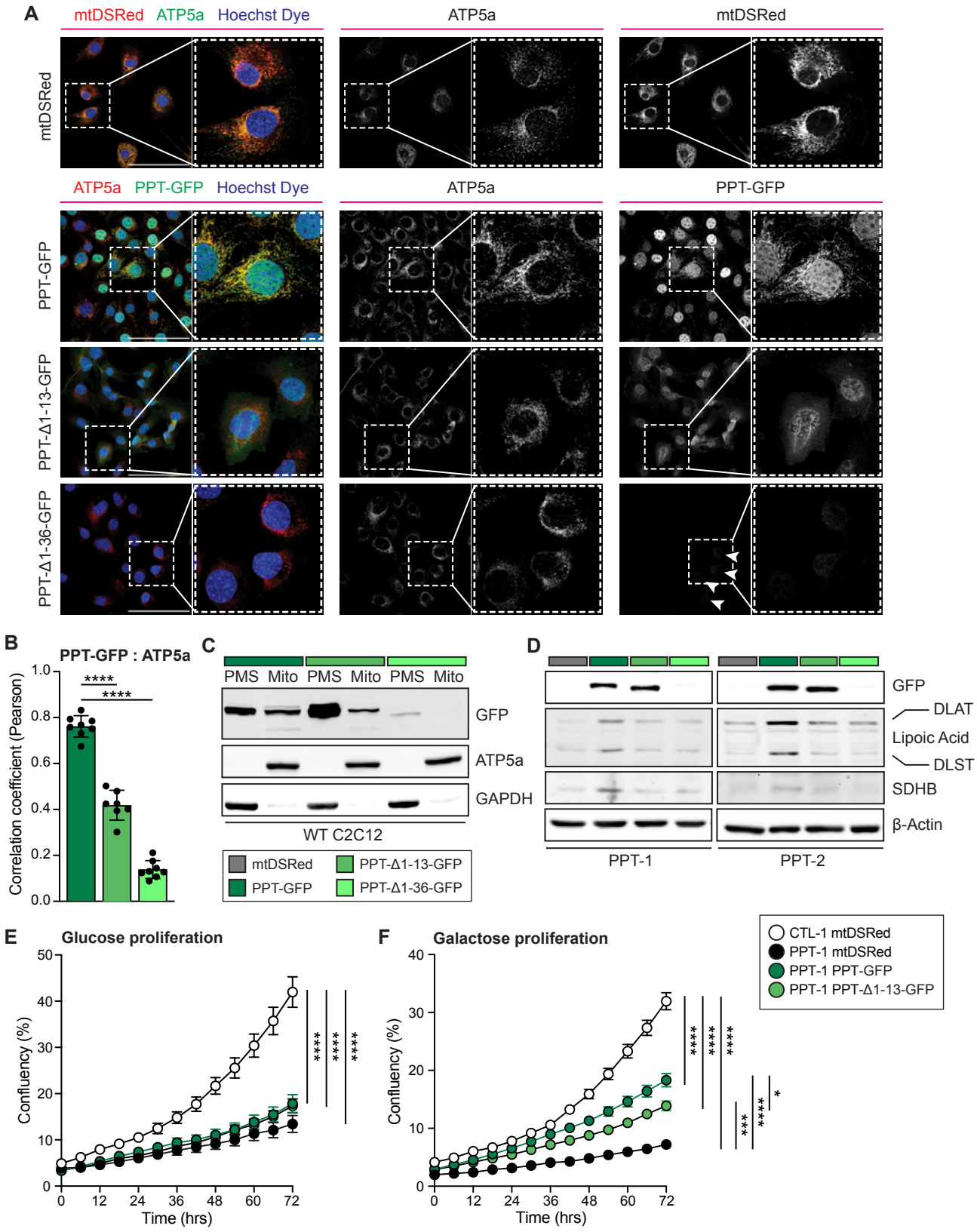
A
mtDSRed ATP5a Hoechst Dye
ATP5a
mtDSRed
mtDSRed
ATP5a PPT-GFP Hoechst Dye
ATP5a
PPT-GFP
PPT-GFP
PPT-Δ1-13-GFP
PPT-Δ1-36-GFP
B
PPT-GFP : ATP5a
Correlation coefficient (Pearson)
1.0
0.8
0.6
0.4
0.2
0.0
****
****
C
PMS Mito PMS Mito PMS Mito
GFP
ATP5a
GAPDH
WT C2C12
mtDSRed
PPT-GFP
PPT-Δ1-13-GFP
PPT-Δ1-36-GFP
D
GFP
DLAT
Lipoic Acid
DLST
SDHB
β-Actin
PPT-1
PPT-2
E
Glucose proliferation
Confluency (%)
Time (hrs)
0 12 24 36 48 60 72
0 10 20 30 40 50
****
****
****
F
Galactose proliferation
Confluency (%)
Time (hrs)
0 12 24 36 48 60 72
0 10 20 30 40
****
****
****
***
****
*
CTL-1 mtDSRed
PPT-1 mtDSRed
PPT-1 PPT-GFP
PPT-1 PPT-Δ1-13-GFP

FIGURE 6

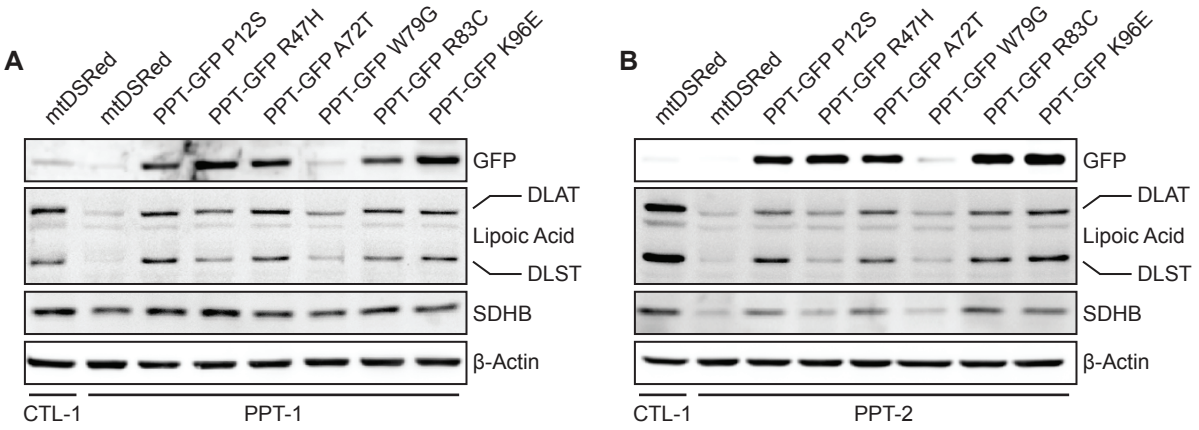
A
mtDSRed
mtDSRed
PPT-GFP P12S
PPT-GFP R47H
PPT-GFP A72T
PPT-GFP W79G
PPT-GFP R83C
PPT-GFP K96E
GFP
DLAT
Lipoic Acid
DLST
SDHB
β-Actin
CTL-1
PPT-1
B
mtDSRed
mtDSRed
PPT-GFP P12S
PPT-GFP R47H
PPT-GFP A72T
PPT-GFP W79G
PPT-GFP R83C
PPT-GFP K96E
GFP
DLAT
Lipoic Acid
DLST
SDHB
β-Actin
CTL-1
PPT-2

FIGURE 1 SUPPLEMENTAL

A **PPT-1/2 mutations**

Cell line	NC_000075.7	Protein
PPT-1	c.342_344delAGC c.398G>C c.478C>G c.479T>G c.739C>T c.740T>G c.744C>T c.745G>T c.752G>A c.754T>A c.758G>A c.764A>T c.767Tdel c.771G>A c.773G>A c.779G>A	p.Q41del p.A60P p.A62G p.R64F p.M66I p.I67K p.L70F p.A72Q p.E73K p.K74N p.L75*
	c.342_346delAGCCG	p.0? (Frameshift)
PPT-2	c.366G>T c.394G>C c.757G>T c.771G>T	p.G49V p.K58N p.R68M p.E73*
	c.342_346delAGCCG	p.0? (Frameshift)

B **Brightfield: Proliferation (72 hrs)**

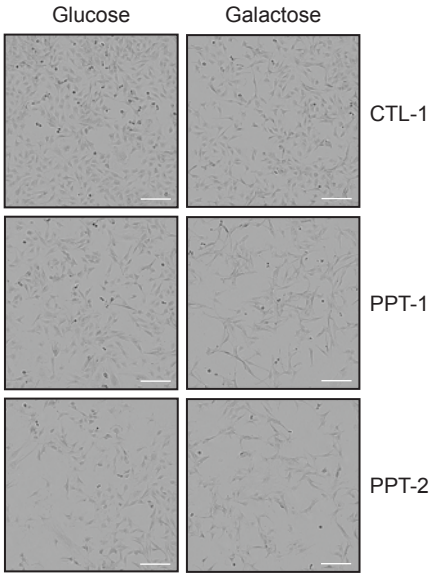

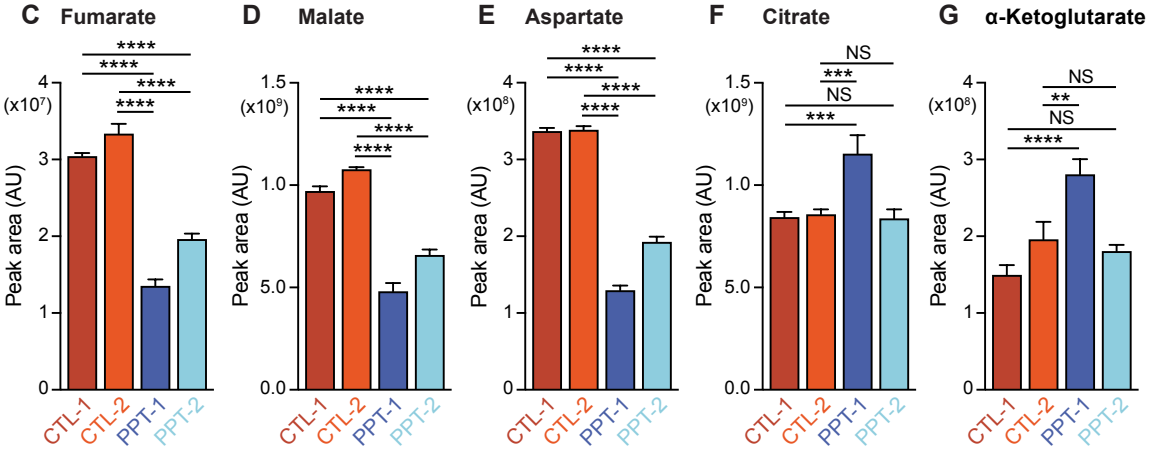

FIGURE 2 SUPPLEMENTAL

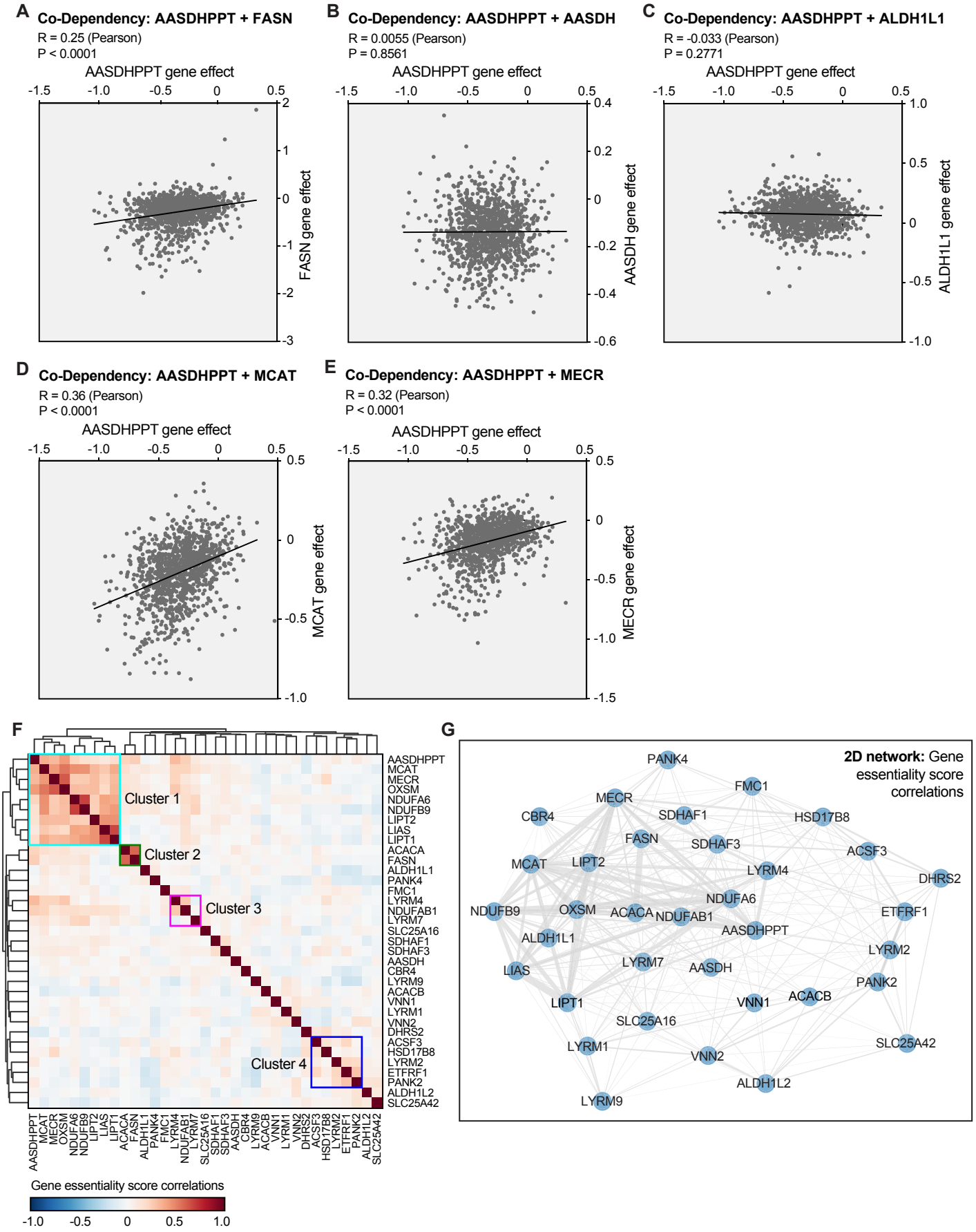

FIGURE 3 SUPPLEMENTAL

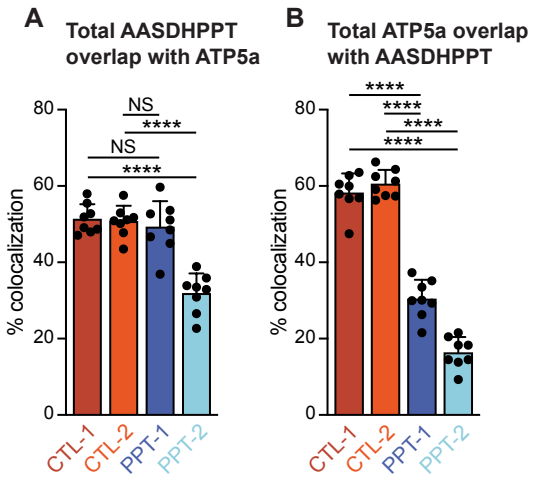

FIGURE 5 SUPPLEMENTAL

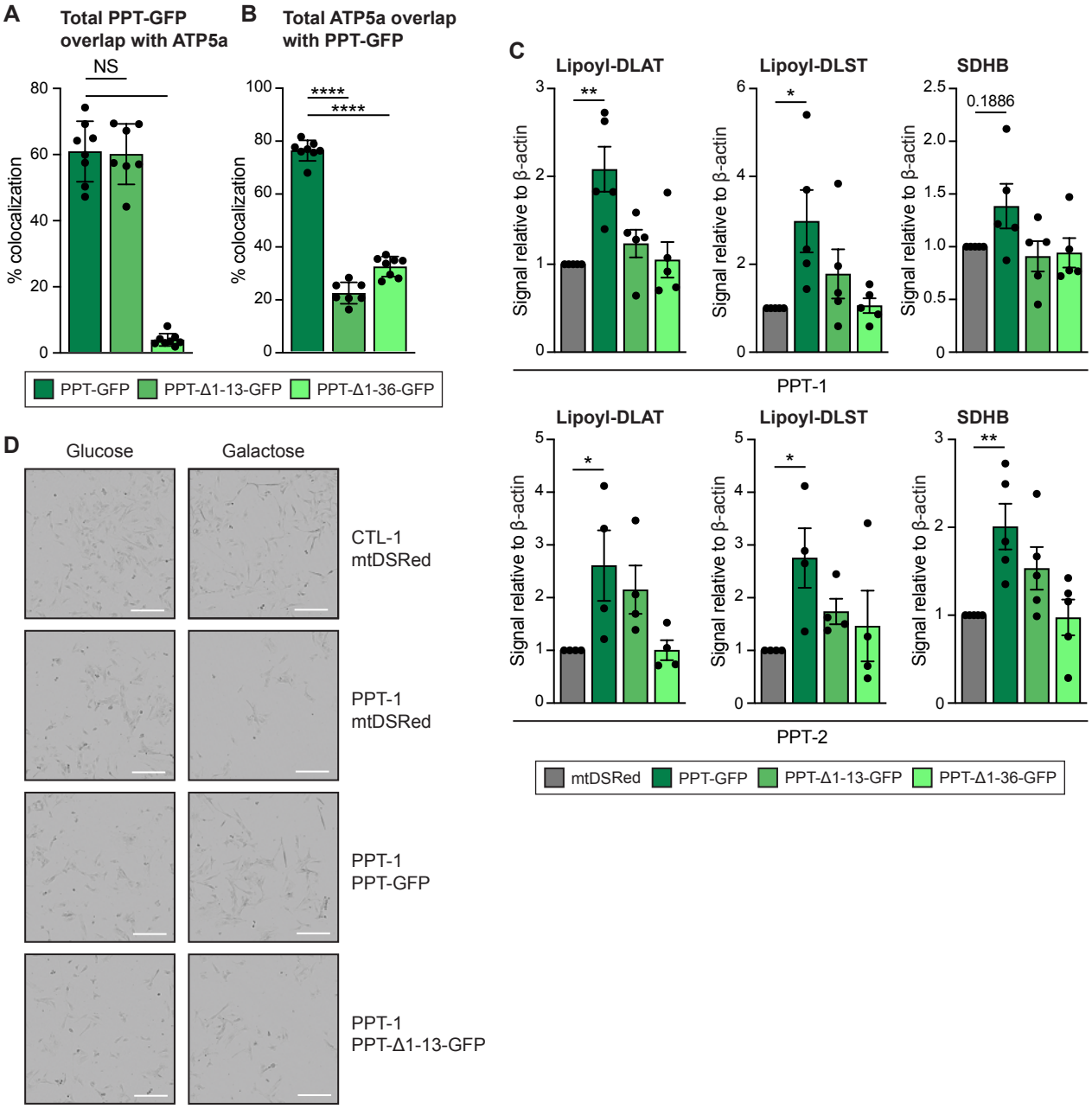

836 **References**

837 1. Shen, Y. *et al.* Mitochondrial ATP generation is more proteome efficient than glycolysis.
838 *Nat. Chem. Biol.* (2024) doi:10.1038/s41589-024-01571-y.
839 2. Yang, H., Ye, D., Guan, K.-L. & Xiong, Y. IDH1 and IDH2 mutations in tumorigenesis:
840 mechanistic insights and clinical perspectives. *Clin. Cancer Res.* **18**, 5562–5571 (2012).
841 3. Beld, J., Sonnenschein, E. C., Vickery, C. R., Noel, J. P. & Burkart, M. D. The
842 phosphopantetheinyl transferases: catalysis of a post-translational modification crucial
843 for life. *Nat. Prod. Rep.* **31**, 61–108 (2014).
844 4. Bar-Peled, L. & Kory, N. Principles and functions of metabolic compartmentalization. *Nat.*
845 *Metab.* **4**, 1232–1244 (2022).
846 5. Zecchin, A., Stapor, P. C., Goveia, J. & Carmeliet, P. Metabolic pathway
847 compartmentalization: an underappreciated opportunity? *Curr. Opin. Biotechnol.* **34**, 73–
848 81 (2015).
849 6. Chen, N., Liu, Y., Li, Y. & Wang, C. Chemical Proteomic Profiling of Protein 4'-
850 Phosphopantetheinylation in Mammalian Cells. *Angew. Chem. Int. Ed Engl.* **59**, 16069–
851 16075 (2020).
852 7. Stuible, H. P., Meier, S., Wagner, C., Hannappel, E. & Schweizer, E. A novel
853 phosphopantetheine:protein transferase activating yeast mitochondrial acyl carrier
854 protein. *J. Biol. Chem.* **273**, 22334–22339 (1998).
855 8. Joshi, A. K., Zhang, L., Rangan, V. S. & Smith, S. Cloning, Expression, and
856 Characterization of a Human 4′-Phosphopantetheinyl Transferase with Broad Substrate
857 Specificity*. *J. Biol. Chem.* **278**, 33142–33149 (2003).
858 9. Van Vranken, J. G. *et al.* ACP Acylation Is an Acetyl-CoA-Dependent Modification
859 Required for Electron Transport Chain Assembly. *Mol. Cell* **71**, 567-580.e4 (2018).
860 10. Nowinski, S. M., Van Vranken, J. G., Dove, K. K. & Rutter, J. Impact of Mitochondrial Fatty
861 Acid Synthesis on Mitochondrial Biogenesis. *Curr. Biol.* **28**, R1212–R1219 (2018).

862 11. Wedan, R. J., Longenecker, J. Z. & Nowinski, S. M. Mitochondrial fatty acid synthesis is
863 an emergent central regulator of mammalian oxidative metabolism. *Cell Metab.* **36**, 36–
864 47 (2024).
865 12. Solmonson, A. & DeBerardinis, R. J. Lipoic acid metabolism and mitochondrial redox
866 regulation. *J. Biol. Chem.* **293**, 7522–7530 (2018).
867 13. Nowinski, S. M. *et al.* Mitochondrial fatty acid synthesis coordinates oxidative metabolism
868 in mammalian mitochondria. *Elife* **9**, e58041 (2020).
869 14. Mullen, A. R. *et al.* Reductive carboxylation supports growth in tumour cells with defective
870 mitochondria. *Nature* **481**, 385–388 (2011).
871 15. Tsherniak, A. *et al.* Defining a cancer dependency map. *Cell* **170**, 564-576.e16 (2017).
872 16. Wainberg, M. *et al.* A genome-wide atlas of co-essential modules assigns function to
873 uncharacterized genes. *Nat. Genet.* **53**, 638–649 (2021).
874 17. DepMap, B. DepMap 23Q4 Public. Figshare+
875 https://doi.org/10.25452/FIGSHARE.PLUS.24667905.V2 (2023).
876 18. Mikolajczyk, S. & Brody, S. De novo fatty acid synthesis mediated by acyl-carrier protein
877 in Neurospora crassa mitochondria. *Eur. J. Biochem.* **187**, 431–437 (1990).
878 19. Sackmann, U., Zensen, R., Röhlen, D., Jahnke, U. & Weiss, H. The acyl-carrier protein
879 in Neurospora crassa mitochondria is a subunit of NADH:ubiquinone reductase (complex
880 I). *Eur. J. Biochem.* **200**, 463–469 (1991).
881 20. Dunn, K. W., Kamocka, M. M. & McDonald, J. H. A practical guide to evaluating
882 colocalization in biological microscopy. *Am. J. Physiol. Cell Physiol.* **300**, C723-42 (2011).
883 21. Kerppola, T. K. Design and implementation of bimolecular fluorescence complementation
884 (BiFC) assays for the visualization of protein interactions in living cells. *Nat. Protoc.* **1**,
885 1278–1286 (2006).
886 22. Omura, T. Mitochondria-targeting sequence, a multi-role sorting sequence recognized at
887 all steps of protein import into mitochondria. *J. Biochem.* **123**, 1010–1016 (1998).

888 23. Webb, B. D. *et al.* Recessive pathogenic variants in MCAT cause combined oxidative
889 phosphorylation deficiency. *Elife* **12**, (2023).
890 24. Landrum, M. J. *et al.* ClinVar: improving access to variant interpretations and supporting
891 evidence. *Nucleic Acids Res.* **46**, D1062–D1067 (2018).
892 25. Bunkoczi, G. *et al.* Mechanism and substrate recognition of human holo ACP synthase.
893 *Chem. Biol.* **14**, 1243–1253 (2007).
894 26. Naquet, P., Kerr, E. W., Vickers, S. D. & Leonardi, R. Regulation of coenzyme A levels by
895 degradation: the “Ins and Outs.” *Prog. Lipid Res.* **78**, 101028 (2020).
896 27. Kastaniotis, A. J., Autio, K. J. & R Nair, R. Mitochondrial fatty acids and neurodegenerative
897 disorders. *Neuroscientist* **27**, 143–158 (2021).
898 28. Lambrechts, R. A. *et al.* CoA-dependent activation of mitochondrial acyl carrier protein
899 links four neurodegenerative diseases. *EMBO Mol. Med.* **11**, e10488 (2019).
900 29. Sanjana, N. E., Shalem, O. & Zhang, F. Improved vectors and genome-wide libraries for
901 CRISPR screening. *Nat. Methods* **11**, 783–784 (2014).
902 30. Rausch, T., Fritz, M. H.-Y., Untergasser, A. & Benes, V. Tracy: basecalling, alignment,
903 assembly and deconvolution of sanger chromatogram trace files. *BMC Genomics* **21**, 230
904 (2020).
905 31. Trefely, S., Ashwell, P. & Snyder, N. W. FluxFix: automatic isotopologue normalization for
906 metabolic tracer analysis. *BMC Bioinformatics* **17**, 485 (2016).
907 32. Meyers, R. M. *et al.* Computational correction of copy number effect improves specificity
908 of CRISPR–Cas9 essentiality screens in cancer cells. *Nat. Genet.* **49**, 1779–1784 (2017).
909 33. Dempster, J. M. *et al.* Extracting biological insights from the project Achilles genome-
910 scale CRISPR screens in cancer cell lines. *bioRxiv* (2019) doi:10.1101/720243.
911 34. Dempster, J. M. *et al.* Chronos: a CRISPR cell population dynamics model. *bioRxiv*
912 (2021) doi:10.1101/2021.02.25.432728.

913 35. Arnold, P. K. *et al.* A non-canonical tricarboxylic acid cycle underlies cellular identity.
914 *Nature* **603**, 477–481 (2022).
915 36. Pacini, C. *et al.* Integrated cross-study datasets of genetic dependencies in cancer. *Nat.*
916 *Commun.* **12**, 1661 (2021).